International Journal of Advanced Multidisciplinary Research and Studies

The Photooxidation of Flavonols and Polyaromatics in Textile Industry Wastewater with La Doped ZnO Nanocomposites and the Evaluation of Acute Toxicity Assays with Microtox and *Daphnia magna*

[1] Rukiye Öztekin, [2] Delia Teresa Sponza

[1, 2] Department of Environmental Engineering, Faculty of Engineering, Tınaztepe Campus, Dokuz Eylül University, Buca, Izmi, Turkey

Corresponding Author: **Rukiye Öztekin**

Abstract

In this study, lanthanum doped zinc oxide (La-ZnO) nanocomposites (NCs) was used for the photocatalytic oxidation of pollutant parameters [COD (chemical oxygen demand) components (COD_{total}, $COD_{dissolved}$, COD_{inert}), flavonols, polyaromatic amines and color] from the effluent of textile industry wastewaters (TI ww) at different operational conditions such as, at increasing photooxidation times (5-15-30-60-80-100 min), at different La mass ratios (0.5wt%, 1wt%, 1.5wt%, 2wt%), at different La-ZnO NCs photocatalyst concentrations (1-5-15-30-45 mg/l), under different ultraviolet (UV) irradiations (10-30-50-100 W/l), at different pH ranges (4.0-6.0-8.0-10.0), respectively. The physicochemical properties of the La-ZnO NCs produced under laboratory conditions were researched using X-Ray Diffraction (XRD) analysis, scanning electron microscopy (SEM) analysis, Fourier Transform Infrared Spectroscopy (FTIR) analysis and UV-visible absorption spectra analysis, respectively. The results were compared with pure ZnO. The maximum COD_{total}, COD_{inert}, total flavonols, total aromatic amines (TAAs) and color photooxidation yields were 99%, 92%, 91%, 98% and 99% respectively, under the optimized conditions, at 30 mg/l La-ZnO NCs with a La mass ratio of 1.5 wt% under 50 W/l UV light, after 60 min photooxidation, at 25ºC at a pH=8.0. The photooxidation yields of kaempferol (KPL), quercetin (QEN), patuledin (PTN), rhamnetin (RMN) and rhamnazin (RHAZ) from flavonols and 2-methoxy-5-methylaniline (MMA), 2,4-diaminoanisole (DAA); 4,40-diamino diphenyl ether (DDE), o-aminoazotoluene (OAAT), and 4-aminoazobenzol (AAB) from polyaromatic amines and their metabolites were > 82% via photodegradation. The pollutants in TI ww were effectively photodegraded with La-ZnO NCs. 94.44% maximum Microtox (with *Aliivibrio fischeri* or *Vibrio fischeri*) acute toxicity yield was found in La-ZnO NCs=10 mg/l after 150 min photooxidation at 60ºC. 90% maximum *Daphnia magna* acute toxicity removal was obtained in La-ZnO NCs=10 mg/l after 150 min photooxidation at 60ºC. La-ZnO NCs concentrations > 10 mg/l decreased the acute toxicity removals by hindering the photooxidation process. Finally, the toxicity originating from the La-ZnO NCs is not significant and the real acute toxicity throughout photooxidation was attributed to the TI ww, to their metabolites and to the photodegradation by-products.

1. Introduction

Textile industry is one of those industries that consume large amounts of water in the manufacturing process (Lin and Chen, 1997) [20] and, also, discharge great amounts of effluents with synthetic dyes to the environment causing public concern and legislation problems. Synthetic dyes that make up the majority (60–70%) of the dyes applied in textile processing industries (Van der Zee *et al.*, 2001) [32] are considered to be serious health risk factors. Apart from the aesthetic deterioration of water bodies, many colorants and their breakdown products are toxic to aquatic life (Chung and Stevens, 1993) [7] and can cause harmful effects to humans (Oliveira *et al.*, 2007) [22]. Several physico-chemical and biological methods for dye removal from wastewater have been investigated (Van der Zee and Villaverde, 2005; Roosta *et al.*, 2014) [33, 26] and seem that each technique faces the facts of technical and economical limitations (Van der Zee and Villaverde, 2005) [33]. The traditional physical, chemical and biologic means of wastewater treatment often have little degradation effect on this kind of pollutants. The TI ww

cannot be treated effectively with concentional treatment processes due to high polyphenols and color content. On the contrary, the technology of nanoparticulate photodegradation has been proved to be effective to them. Compared with the other conventional wastewater treatment means, this technology has such advantages as: (1) wide application, especially to the molecule structure-complexed contaminants which cannot be easily degraded by the traditional methods; (2) the nanoparticles (NPs) itself have no toxicity to the health of our human livings and (3) it demonstrates a strong destructive power to the pollutants and can mineralize the pollutants into carbondioxide (CO_2) and water (H_2O) (Tavakkoli and Moayedipour, 2014) [31]. Semiconductor photocatalysis is an advanced oxidation process (AOP) for the treatment of wastewater streams (Huang, 2008). ZnO, a II–VI compound semiconductor with a wide direct band gap (3.37 eV) and a large exciton binding energy (60 meV) at room temperature, has attracted increasing attention due to its excellent properties through applications in photocatalysts (Li *et al*., 2007) [19]. As a photocatalyst, the destruction ability of ZnO and ZnO based materials starts with absorption of light energy equal or greater than the band-gap energy and continues with the generation of electron–hole pairs (Senthilvelan *et al*., 2012) [28]. Then, these charge carriers can be separately trapped by the oxygen (O_2) and surface hydroxyl (OH) groups to produce primary oxidizing species; hydroxyl radicals ($OH^•$). The subsequent attacks of the radicals to surface adsorbed pollutants yield mineralized species. The higher efficiency of ZnO has been reported in several studies such as photocatalytic oxidation of phenol (Marci *et al*., 2001) [21], 2-phenly phenol (Khodja *et al*., 2001) [17], acid red 18 (Sobana and Swaminathan, 2007) [29], remazol brilliant blue R, remazol black B, reactive blue 221 and reactive blue 222 (Gouvea *et al*., 2000) [12].

In order to reduce the recombination rate of ZnO in the photocatalytic processes some alkaline and rare earth metal atoms can be doped on the surface of the semiconductors, which have been shown to reduce band gap energy and improve charge separation between photogenerated electrons and holes (Pareek and Adesina, 2003) [24]. Recently, Anandan *et al*. (2007a) [2] found 80% monocrotophos removal efficiency during photooxidation at

a power of 64 W using 25 g/l La-ZnO with a La mass ratio of 0.8 wt% after 120 min. It was found that La-doped ZnO showed higher photocatalytic activity in the degradation of monocrotophos as compared to that of pure ZnO and TiO_2 (Anandan *et al*., 2007a) [2]. When 0.6wt% La mass ratio was doped into ZnO, more surface defects are produced, which hindered the recombination of photo-induced electron–hole pairs (Anandan *et al*., 2007b) [3]. Byrappa *et al*. (2006) [5] and Sobana and Swaminattan (2007) [29] investigated the photoooxidation of Rhodamine B and Acid-Red 18 from TI ww using nano-ZnO. The photodegradation studies performed with La doped ZnO to remove some dyes from TI ww are limited only with few studies: Jia *et al*. (2009) [14], Suwanboon *et al*. (2013) [30] and Kaneva *et al*. (2015) [16] used nano La doped ZnO to treat the Rhodamine B, Metilen blue and azo dyes.

No study was found investigating the pollutants (COD, the flavonols and polyaromatic amines) from TI ww with La doped ZnO and the evaluation of acute toxicity assays for the photodegradation experimental results. Therefore, in the present study, La-ZnO NCs was used for the photocatalytic oxidation of pollutant parameters [COD components (COD_{total}, $COD_{dissolved}$, COD_{inert}), flavonols (kaempferol, quercetin, patuledin, rhamnetin and rhamnazin), polyaromatic amines (2-methoxy-5-methylaniline, 2,4-diaminoanisole, 4,40-diamino diphenyl ether, o-aminoazotoluene, and 4-aminoazobenzol) and color] from the TI ww at different operational conditions such as, at increasing photooxidation times (5 min, 15 min, 30 min, 60 min, 80 min and 100 min), at diferent La mass ratios (0.5wt%, 1wt%, 1.5wt%, 2wt%), at different La doped-ZnO photocatalyst concentrations (1 mg/l, 5 mg/l, 15 mg/l, 30 mg/l and 45 mg/l), at different pH ranges (4.0, 6.0, 8.0 and 10.0) under different UV light irradiations (10 W/l, 30 W/l, 50 W/l and 100 W/l), respectively. In addition to, the acute toxicity assays was examined with Microtox (with *Vibrio Fischeri*) and *Daphnia magna* at the photodegradation experimental results with La doped ZnO NCs in TI ww.

2. Materıal and methods
2.1 Raw Wastewater
The characterization of raw TI ww was given in Table 1.

Table 1: Characterization values of TI ww at pH=5.7 (n=3, mean values ± SD). (SD: standard deviation; n: the repeat number of experiments in this study)

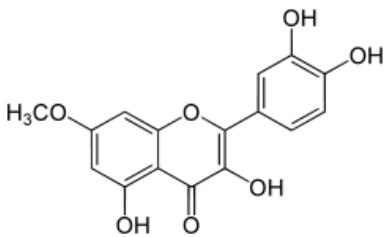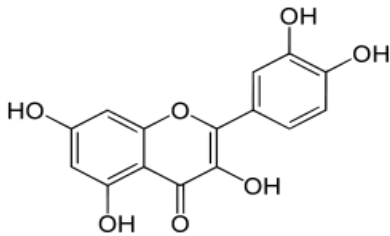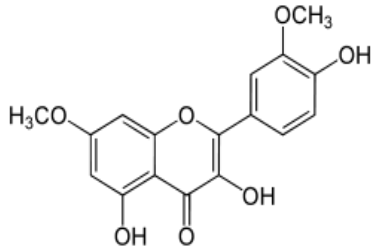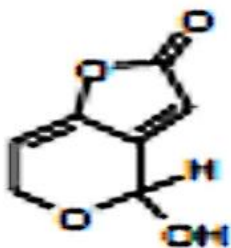| Parameters	Values		
	Minimum	**Medium**	**Maximum**
pH	5.00 ± 0.18	5.27 ± 0.19	6.00 ± 0.21
DO (mg/l)	1.30 ± 0.05	1.40 ± 0.05	1.50 ± 0.05
ORP (mV)	85.00 ± 2.98	106.00 ± 3.71	128.00 ± 4.48
TSS (mg/l)	285.00 ± 9.98	356.00 ± 12.46	430.00 ± 15.05
TVSS (mg/l)	192.00 ± 6.72	240.00 ± 8.40	290.00 ± 10.15
COD_{total} (mg/l)	931.70 ± 32.61	1164.60 ± 40.76	1409.20 ± 49.32
$COD_{dissolved}$ (mg/l)	770.40 ± 26.96	962.99 ± 33.71	1165.22 ± 40.78
TOC (mg/l)	462.40 ± 16.18	578.00 ± 20.23	700.00 ± 24.50
BOD_5 (mg/l)	251.50 ± 8.80	314.36 ± 11.00	380.38 ± 13.31
BOD_5/COD_{dis}	0.26 ± 0.01	0.33 ± 0.012	0.40 ± 0.014
Total N (mg/l)	24.80 ± 0.87	31.00 ± 1.09	37.51 ± 1.31
NH_4-N (mg/l)	1.76 ± 0.06	2.20 ± 0.08	2.66 ± 0.09
NO_3-N (mg/l)	8.00 ± 0.28	10.00 ± 0.35	12.10 ± 0.42
NO_2-N (mg/l)	0.13 ± 0.05	0.16 ± 0.06	0.19 ± 0.07
Total P (mg/l)	8.80 ± 0.31	11.00 ± 0.39	13.30 ± 0.47
PO_4-P (mg/l)	6.40 ± 0.22	8.00 ± 0.28	9.68 ± 0.34
SO_4^{-2} (mg/l)	1248.00±43.70	1560.00 ± 54.60	1888.00 ± 66.10
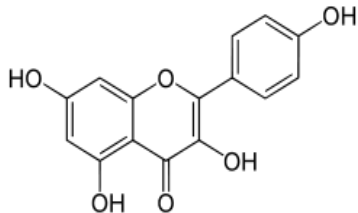
Color (1/m)	70.90 ± 2.48	88.56 ± 3.10	107.20 ± 3.75
Total Flavonols (mg/l)	30.9 ± 1.08	38.6 ± 1.35	46.1 ± 1.61
Flavonols concentrations (mg/l)			
Kaempferol	4.2 ± 0.20	5.7 ± 0.2	7.2 ± 0.3
Quercetin	7.3 ± 0.26	9.2 ± 0.32	11.1 ± 0.4
Patuledin	8.3 ± 0.30	10.3 ± 0.36	12.2 ± 0.43
Rhamnetin	6.0 ± 0.21	7.2 ± 0.25	8.4 ± 0.3
Rhamnazin	5.1 ± 0.18	6.15 ± 0.22	7.2 ± 0.25
TAAs (mg benzidine/l)	891.84 ± 31.21	1038 ± 36.3321	1183.8±41.4321
Polyaromatics concentrations (mg/l)			
2-methoxy-5-methylaniline	128.5 ± 4.5	134.6 ± 4.71	140.6 ± 4.92
2,4-diaminoanisole	250.2 ± 8.76	275.8 ± 9.7	301.3 ± 10.6
4,40-diamino diphenyl ether	146.54 ± 5.13	156.0 ± 5.5	165.4 ± 5.8
o-aminoazotoluene	265.4 ± 9.3	293.6 ± 10.3	321.7 ± 11.3
4-aminoazobenzol	101.2 ± 3.54	178 ± 6.23	254.8 ± 8.92

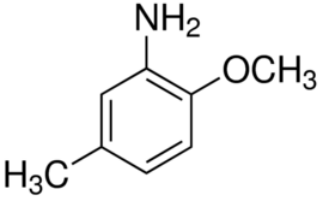## 2.2 Chemical Structure of Flavonols and Poliaromatics Present in the TI ww
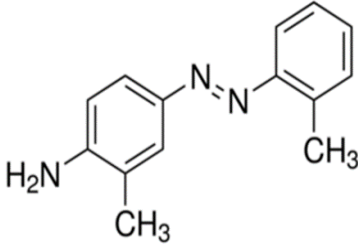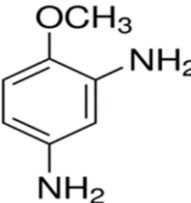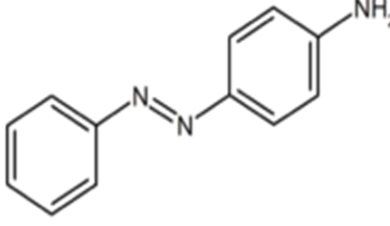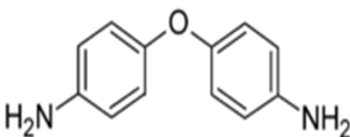
The structure of flavonols in the TI ww was shown in Fig 1. The structure of polyaromatics in the TI ww was given Fig 2.

Fig 1: Chemical structure of flavonoids in the TI ww

Chemical structure of flavonoids	Chemical structure of flavonoids
kaempferol	rhamnetin
quercetin	rhamnazin
patuledin	

Fig 2: Chemical structure of polyaromatics in the TI ww

Chemical structure of polyaromatics	Chemical structure of polyaromatics
 2-methoxy-5-methylaniline	 o-aminoazotoluene
 2,4-diaminoanisole	 4-aminoazobenzol
 4,40-diamino diphenyl ether	

2.3 Preparation of La-ZnO NPs Photocatalysts

La-ZnO NPs were prepared by co-precipitation method using zinc nitrate hexahydrate $[Zn(NO_3)_2.6H_2O]$ (Analytical grade, Merck) and lanthanum nitrate hexahydrate $[La(NO_3)_3 \cdot 6H_2O]$ (Sigma, Aldrich) as the precursors of Zn^{+2} and La^{+3}, respectively. $Zn(NO_3)_2.6H_2O$ and sodium carbonate anhydrous (Na_2CO_3) were dissolved separately in double distilled H_2O to obtain 0.5 mol/l solutions. Lanthanum nitrate $[La(NO_3)_3]$ in the required stoichiometry was slowly added into the above solution and a white precipitate was obtained. The precipitate was filtered, repeatedly rinsed with distilled H_2O and then washed twice with ethanol. The resultant solid product was dried at 100ºC for 12 h and calcined at 300ºC for 2 h. The doped La mass ratios of La^{+3} are expressed as wt%.

2.4 X-Ray Diffraction (XRD) Analysis

XRD analysis were performed using powder diffraction method. The NCs powder was pressed into a pellet by using a diluent namely KBr. XRD patterns of the samples are going to carry out using a D/Max-2400Rigaku X-ray powder diffractometer operated in the reflection mode with Cu Ka (λ = 0.15418 nm) radiation through scan angle (2θ) from 20º to 80º.

2.5 Scanning Electron Microscopy (SEM) Analysis

The morphological structures of the La-ZnO NCs before photocatalytic degradation with UV light irradiations and after photocatalytic degradation with UV by means of a SEM analysis measurements.

2.6 Fourier Transform Infrared Spectroscopy (FTIR) Analysis

The FTIR spectra of La, ZnO and La-ZnO samples were measured with FTIR spectroscopy measurements.

2.7 Photocatalytic Degradation Reactor

A 2 liter cylinder quartz glass reactor was used for the photodegradation experiments in the TI ww under different UV powers, at different operational conditions. 1000 ml TI ww was filled for experimental studies and the photocatalyst were added to the cylinder quartz glass reactors. The UV-A lamps were placed to the outside of the photo-reactor with a distance of 3 mm. The photocatalytic reactor was operated with constant stirring (1.5 rpm) during the photocatalytic degradation process (Fig 3). 10 ml of the reacting solution were sampled and centrifugated (at 10000 rpm) at different time intervals. The UV irradiation treatments were created using one or three UV-A lamp emitting in the 350–400 nm range (λ_{max} = 368 nm; FWHM = 17 nm; Actinic BL TL-D 18W, Philips).
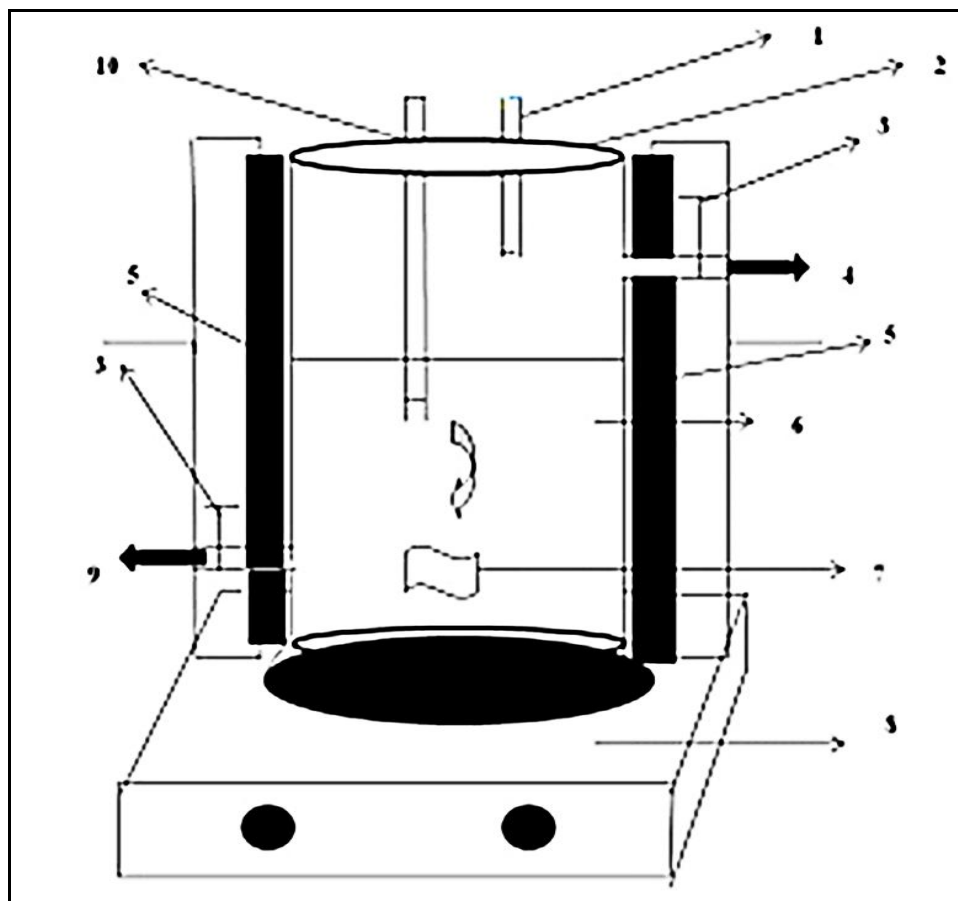
Fig 3: Photodegradation experimental scheme (1: thermometer, 2: teflon proofed cover, 3: proofed tap, 4: gas sampling inlet, 5: UV light sources (OSRAM Germicidal Hg lamb, 30 W UV-C lamb), 6: 1000 ml kuvars glass reactor, 7: magnetic fish, 8: magnetic stirrer, 9: liquid sampling inlet, 10: pH meter.

2.8 Used chemicals

$Zn(NO_3)_2.6H_2O$ (Analytical Grade, Merck, Germany) and $La(NO_3)_3 \cdot 6H_2O$ (Analytical grade, Merck, Germany) were used as Zn^{+2} and La^{+3} sources, respectively. Na_2CO_3 was purchased from Merck (Analytical grade). Helium, He(g) (GC grade, 99.98%) and nitrogen, $N_2(g)$ (GC grade, 99.98%) was purchased from Linde, (Germany). Kaempferol (99%), quercetin (99%), patuledin (99%), rhamnetin (99%), rhamnazin (99%), 2-methoxy-5-methylaniline (99%), 2,4-diaminoanisole (99%), 4,40-diamino diphenyl-ether (99%), o-aminoazotoluene (99%), 4-aminoazobenzol (99%), 3-*O*-[2-*O*,6-*O*-Bis(α-L-rhamnosyl)]-β-D--glucosyl]kaempferol (99%), 3-O-[2-O, 6-O-bis (¬-l-rhamnosyl)-(3-d-glucosyl] kaempferol (99%), 3-*O*-[6-*O*-(¬-l-rhamnosyl)-(3-d- glucosyl] kaempferol (99%), 3-*O*-[2-*O*, 6-*O*-bis (¬-l-rhamnosyl)-(3-d-glucosyl) quercetin (99%), 3-*O*-{2-*O*-[6-*O*-(*p*-hydroxy-*trans*-cinnamoyl)-(*ß*-D -glucosyl]-- *á*-L- rhamnosyl} quercetin (99%), (E)-ascladiol (99%), (Z)-ascladiol (99%), Methyl quercetin (99%), Tetrahydroxy-7-methoxyflavone (99%), Rham nazin-3-0-ß-D -glucopyranosyl-(l →5)- *α*-L-arabinofuranoside (99%), Rhamnazin-3-O-ß-D- glucopyranosyl-(l—»5)-[ß-D-apiofuranosyl-(-1→2)]-*α* -L-arabinofuranoside (99%), 5-nitro-o-toluidine (99%), 4-acetylamino-2-aminoanisole (99%), 2,4-diacetylaminoanisole (99%), N,N*l*-diacetyl-4,4*l*-diaminobenzhydrol (99%), N,N*l*-diacetyl-4,4 *l* – diaminophenylmethane (99%), hydroxy-OAT (I) (99%), 4′ - hydroxy-OAAT (99%), 2′ -hydroxymethyl-3-methyl-4-aminoazobenzene (99%), 4, 4′-bis(otolylazo)-2, 2′ - dimethylazoxybenzene (99%), Phenylhydroxylamine (99%), and Nitrosobenzol (99%) were purchased from Aldrich, (Germany).

2.9 Analytical methods

pH, T(ºC), ORP, DO, BOD_5, COD_{total}, $COD_{dissolved}$, total suspended solids (TSS), Total-N, NH_3-N, NO_3-N, NO_2-N, Total-P and PO_4-P measurements were monitored following the Standard Methods 2310, 2320, 2550, 2580, 4500-O, 5210 B, 5220 D, 2540 D, 4500-N, 4500-NH₃, 4500-NO₃, 4500-NO₂ and 4500-P (Baird *et al.*, 2017) [4]. Inert COD was measured according to glucose comparison method (Germirli *et al.*, 1991) [11]. The samples were analyzed by high performance (or pressure) liquid chromatography (HPLC) with photodiode array and mass spectrometric detection (MSD) using an Agilent 1100 HPLC system consisting of an automatic injector, a gradient pump, a Hewlett–Packard series 1100 photodiode array detector, and an Agilent series 1100 VL on-line atmospheric pressure ionization electrospray ionization mass spectrometer to detect flavonols namely kaempferol, quercetin, patuledin, rhamnetin, rhamnazin and polyaromatics namely, 2-methoxy-5-methylaniline, 2,4-diaminoanisole, 4,40-diamino diphenyl-ether, o-aminoazotoluene, 4-aminoazobenzol, respectively. All the metabolites were measured in the same HPLC by MSD. Operation of the system and data analysis were done using ChemStation software, and detection was generally done in the negative ion $[M − H]^-$ mode, which gave less complex spectra, although the positive ion mode was sometimes used to reveal fragmentation patterns-especially patterns of sugar attachment. Separation of

flavonol and poliaromatic amines and their metabolites were made on a Vydac C18 reversed phase column (2.1 μm dia. × 250 mm long; 5-μm particle size). Columns were eluted with acetonitrile-water gradients containing 0.1% formic acid in both solvents.

2.10 Adsorption of TW over ZnO and La-doped ZnO

Prior to photocatalytic experiments, adsorption experiments under dark conditions were carried out with 100 ml TI ww over ZnO and La-doped ZnO catalysts. The TW was stirred on a magnetic stirrer and the aliquots were withdrawn at regular intervals for analysis. There is 2% adsorption of COD over La-doped ZnO whereas it is only 0.5% over ZnO (data not shown). All La-doped ZnO catalysts show sligthly higher adsorption capacities than ZnO. The adsorption of COD in TI ww is also an important factor for photocatalytic activity.

2.11 Operational conditions

Under 10-30-50 and 100 W/l UV light powers the photocatalytic oxidation of the pollutant parameters in the TI ww at different operational conditions such as at increasing La mass ratios in the La-ZnO NCs (0.5wt%, 1wt%, 1.5wt% and 2wt%), at increasing photooxidation times (5 min, 15 min, 30 min, 60 min, 80 min and 100 min), at different La-ZnO photocatalyst concentrations (1 mg/l, 5 mg/l, 15 mg/l, 30 mg/l and 45 mg/l), under acidic, neutral and basic conditions such as different pH ranges (4.0-6.0-8.0-10.0), respectively.

All the experiments were carried out following the batch-wise procedure. All experiments were carried out three times and the results were given as the means of triplicate sampling with standard deviation (SD) values.

3. Results and discussion
3.1 XRD Analysis results

Fig 4 shows the XRD patterns of increasing doped La to ZnO. The NPs recorded in the range of 20–70 degree for different La loadings. The XRD patterns of all the La-ZnO catalysts are almost similar to that of ZnO, suggesting that there is no change in the crystal structure upon La loading. In other words, the observed diffraction peaks of the pure ZnO catalyst can be indexed to those of hexagonal wurtzite ZnO (PCPDF79-0207). This also indicates that La^{+3} is

uniformly dispersed on ZnO NPs in the form of small La_2O_3 cluster. No special peaks of impurity phases such as Zn or $Zn(OH)_2$ were observed. As can be seen from Fig 4, there is no diffraction peaks originating from lanthanum, and it's compounds in the XRD data up to an addition of 45 mg/l La to La-ZnO NCs. The absence of La_2O_3 as separate phase might be due to the dissolution of lanthanide in ZnO lattice.
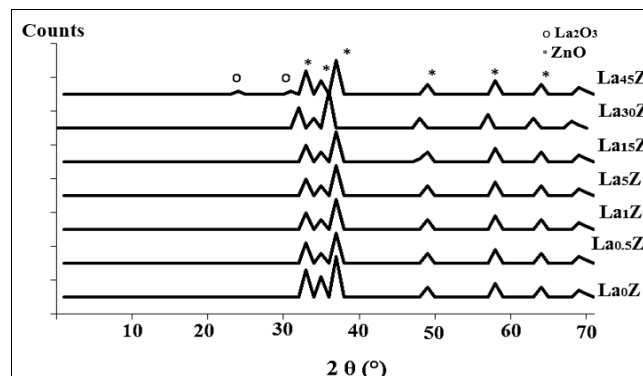

Fig 4: XRD patterns of increasing La concentrations doped on ZnO (Z)

From Fig 5, it can be seen that doping of La makes the XRD peak getting wider compared with pure ZnO. To study the effect of doping on the crystallinity of the ZnO NPs, the intensity of the (100), (002), and (101) diffraction peaks was monitored. The intensities of (100), (002), and (101) diffraction peaks were measured as 2200 au, 1700 au, 3004 au, respectively, for 0 mg/l La (Pure nano-ZnO). The intensity of (100), (002) and (101) diffraction peaks decreased from 2200 au to 1350 au; from 1700 au to 100 and from 3004 au to 1305 au in the presence of 1 mg/l La. The maximum diffraction peaks were measured as 1500 au, 1370 au and 1250 au for 30 mg/l La. As the La doped concentration was increased from 1 mg/l to 30 mg/l in the La-ZnO NCs the XRD peaks increased and getting wider (Fig 5). The width of peak did not increase at 45 mg/l La and the intensities of (100), (002) and (101) diffraction peaks were measured as 1700, 1395 and 1490 au. The changes in the peak for crystallinity might be the result of changes in the atomic environment due to impurity doping on ZnO samples as reported by Raza *et al*. (2014) [25].
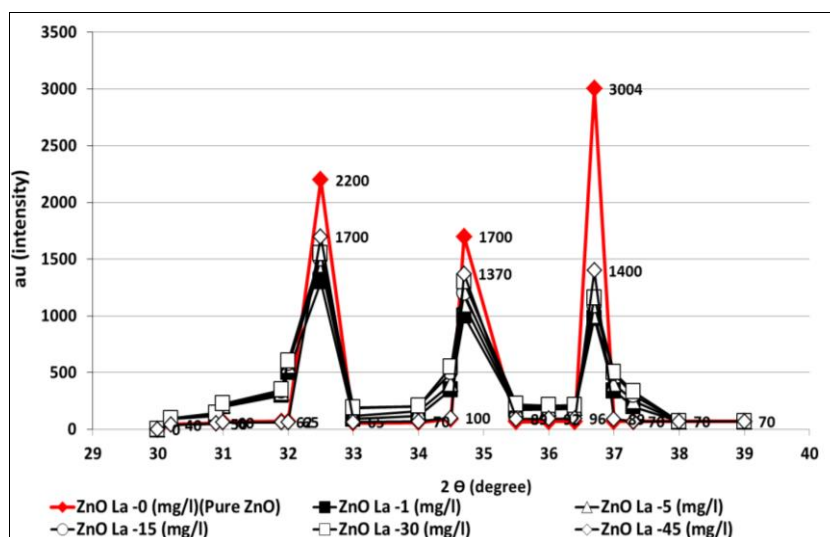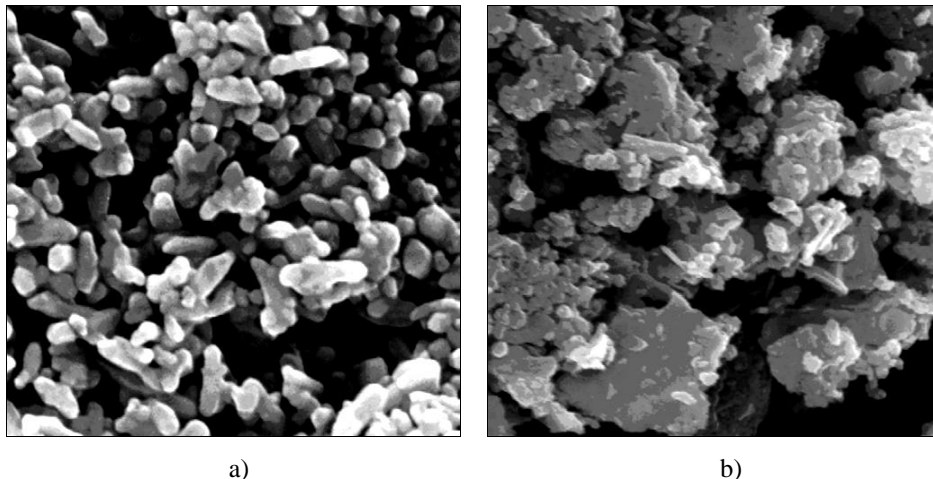

Fig 5: Effects of increasing La doped ratios on the intensities of XRD diffraction peaks in the La-ZnO NCs
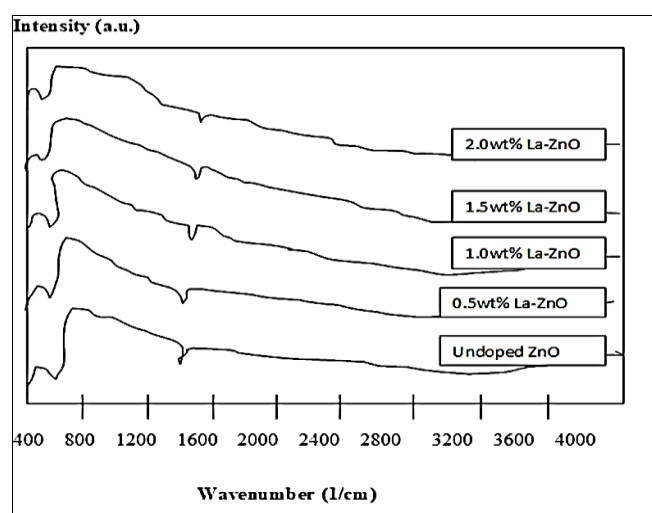
3.2 SEM Analysis results

The morphology of nanocomposite particles is analyzed by SEM. Fig 6 shows that the NCs material is partly composed of clusters containing composite NPs adhering to each other with a mean size of around 20-80 nm before photooxidation process (Fig 6a) while the size was not changed after photooxidation (20.05-80.07 nm) (Fig 6b). The grains with regular shape are visible and the structure appear porous.

The incorporation of La^{+3} did not affect the general microstructure and did not significantly affect the grain growth of these materials. This strongly suggests that the ZnO lattice was not severely disrupted by the La^{+3} ions. The formation of La_2O_3 was not observed from the SEM micrograph that shows different morphology clusters not adhered to the grains and it was shown a rough and pore surface.

| a) | b) |

Fig 6: SEM micrographs of pure and lanthanum modified ZnO, (a) pure ZnO at 25°C, (b) La-ZnO NCs at 25°C

3.3 FTIR Analysis results

Fig 7 shows The FTIR spectrum of 25 mg/l ZnO and 25 mg/l La-ZnO NCs concentrations with four different La mass ratios (0.5wt%, 1wt%, 1.5wt% and 2wt%) in the La-ZnO NCs. The adsorption bands at 412 and 595 1/cm are attributed to the Zn-O stretching vibration of wurtzite hexagonal type ZnO crystal, belonging to the oxygen (O_2) sub-lattice vibration and O_2 vacencies of wurtzite ZnO crystal. The band at 1395 1/cm is specified as hydrogen (H_2)-related defects on surface of ZnO. The broad adsorption bands at 3013-3659 1/cm are the O-H stretching vibration of adsorbed water (H_2O) on ZnO surface.

shifted to shorter wavelength than that ZnO alone. As the La doping increased the UV absorbances decreased. The shifting of absorbance maximum towards shorter wavelength was also reported by Ganesh *et al.* (2012) [10]. This is attributed to quantum size effects. In addition to quantum size effect, appropriate interaction between surface oxidic site of ZnO and La^{3+} may also be the cause for shift of wavelength. The absorbance maxima for all the catalysts and the corresponding band gap values and the rate constants for the degradations of kaempferol from flavonols and for 2-methoxy-5-methylaniline from polyaromatic amines are presented in Table 2. There are gradual increase in the bandgap and in the λ_{max} levels with increase in La loading. The maximum photodegradation rate constants for kaempferol and for 2-methoxy-5-methylaniline were found to be 7.99 x 10^{-2} 1/min and 7.21x10^{-2} 1/min at 1.5 wt% La ratio in the La-ZnO NCs (Table 2).
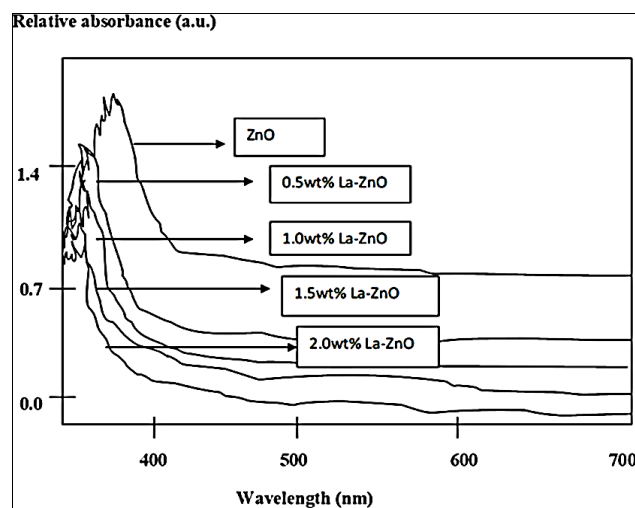

Fig 7: FTIR spectrum of 25 mg/l ZnO and 25 mg/l La-ZnO concentrations with four different La mass ratios (0.5wt%, 1wt%, 1.5wt% and 2wt%) in the La-ZnO NCs

Fig 8: Absorbance maxima of pure ZnO and increasing ratios La-ZnO NCs

3.4 UV-visible Analysis of ZnO and La doped ZnO NCs

The UV-visible absorption spectra of ZnO and La-ZnO are shown in Fig 8. The UV-visible spectra of La-ZnO NCs are

Table 2: UV-vis absorption data for ZnO and La-ZnO catalysts and photodegradation rate constants for kaempferol and 2-methoxy-5-methylaniline

Nanomaterials	λ_{max} (nm)	Band gap (eV)	Photodegradation rate constant, k (x 10-2 1/min)	
			Flavonols (for kaempferol)	Polyaromatic amines (for 2-methoxy-5-methylaniline)
ZnO	390	3.80	3.05	2.24
0.5 wt% La-ZnO	376	3.30	5.99	4.78
1 wt % La-ZnO	375	3.31	6.13	5.99
1.5 wt% La-ZnO	374	3.32	7.99	7.21
2.0 wt % La-ZnO	369	3.37	3.01	2.21

3.5 Effect of Increasing La-ZnO NCs Concentrations on the Removals of TI ww Pollutants

The effects of increasing La-ZnO NCs concentrations (1.0, 5.0, 15, 30 and 45 mg/l), on the photocatalytic oxidation of polutant parameters in the TI ww was investigated. The preliminary studies showed that the maximum removal of COD at La-ZnO NCs=20 mg/l, at a La ratio of 1.5wt% was 89% after 70 min photooxidation time, at pH=7.8 and at 40 W/l UV power, respectively (data not shown). Based on these yields the operational conditions for photocatalytic time were choosen as 60 min, at 50 W/l UV power and at pH=8.0, respectively. The maximum photocatalytic oxidation removals for all pollutants in the TI ww were observed at La-ZnO NCs=30 mg/l with a La ratio of 1.5wt% in the La-ZnO NCs at pH=8.0, after 60 min photooxidation time, at 50 W/l and at 25ºC, respectively (Table 3). Removal efficiencies slightly decreased at La-ZnO NCs=45 mg/l, because over load of surface area of La-ZnO NCs (Table 3).

Table 3: Effect of increasing La-ZnO NCs concentrations with a La ratio of 1.5wt% on the TI ww during photooxidation process after 60 min, at 50 W/l UV irradiation, at pH=8.0 and at 25ºC, respectively

Parameters	Removal efficiencies (%)				
	La-ZnO NCs concentrations (mg/l)				
	1 mg/l	5 mg/l	15 mg/l	30 mg/l	45 mg/l
COD_{total}	51	65	84	99	79
COD_{inert}	45	63	78	92	76
$COD_{dissolved}$	50	64	82	98	80
Color	62	69	85	99	83
Total flavonols	40	58	79	91	72
Flavonols					
Kaempferol	35	57	72	87	65
Quercetin	36	61	73	88	67
Patuledin	37	62	79	90	74
Rhamnetin	38	56	72	87	64
Rhamnazin	34	53	71	85	66
TAAs	58	75	81	98	77
Polyaromatics					
2-methoxy-5-methylaniline	55	66	83	93	79
2,4-diaminoanisole	54	71	79	95	73
4,40-diamino diphenyl ether	52	58	68	87	63
o-aminoazotoluene	49	65	75	84	72
4-aminoazobenzol	47	62	76	82	70

This limiting the power of UV irradiation. Lower photo-removal efficiencies was measured for 1 mg/l, 5 and 15 mg/l La-ZnO NCs concentrations due to low surface areas in the NCs. The results from BET (Brunauer–Emmett–Teller)

analysis of annealed at 100ºC samples are shown in Table 4. With the increase in concentration of La^{+3} ions, the penetration depth of light into ZnO can greatly exceed the space charge layer. Therefore, an optimum concentration of La^{+3} ions is required to match the thickness of charge layer and the depth of the light penetration for separating photoinduced electron–hole pairs. In addition, appropriate loading of La^{+3} ions is highly necessary for producing a significant potential difference between the surface and the center of the particles in order to efficiently separate the photoinduced electron–hole pairs. The maximum photodegradation yield was observed at La-ZnO NCs=30 mg/l concentration. The studies performed by Suwanboon *et al.* (2013) [30] and by Raza *et al.* (2014) [25] showed that addition of an optimum La^{+3} concentration of 5 mg/l to ZnO NCs increased the yields of some dyes (Rhodamine-B, Coomassie Brilliant Blue G250, Acid Green 25) from 23% to 58% after 120 min irradiation time, at 500 W/l UV light irradiation, at 25ºC after this La^{+3} concentration the yield photo-removals decreased.

Table 4: Specific surface area according to BET (Brunauer–Emmett–Teller) analysis

La-modified ZnO samples (mg/l)	Surface area, (m^2/g ± 3%)
1	23.68
5	25.97
15	30.19

The COD_{total}, COD_{inert}, flavonols, aromatic amines and color removals increased as the La-ZnO NCs concentrations were increased from 1 mg/l up to 5 mg/l, to 15 mg/l, and up to 30 mg/l, respectively (Table 3). Furher increase of NCs concentration to 45 mg/l affect negatively all the pollutant yields. The reason for this is the optimum amount of catalyst increases the number of active sites on the photocatalyst surface, which in turn increase the number of OH$^\bullet$ and superoxide radicals (O$_2$ $^-$ $^\bullet$) to degrade pollutant parameters (COD components, flavonols, polyaromatics, color). Excess catalyst cause turbidity, prevent the illumination of light and OH$^\bullet$ productions. Maximum COD_{total}, COD_{inert}, total flavonols, TAAs and color removal efficiencies were obtained after 60 min photooxidation process with yields > 92% at the same operational conditions mentioned above (Table 3). 20 and 30 mg/l ZnO alone exhibited low COD yields (45%, data not shown). The color yields obtained in our study (99%) for TI ww are higher than the studies of Suwanboon *et al.* (2013) [30] and Kaneva *et al.* (2015) [16] (80%) who they investigated the effects of Zn $_{0.95}$La $_{0.05}$O on the treatment of Methylene Blue and Reactive Black 5 under 90 W UV irradiation power for 60 min irradiation time, respectively.

3.6 Identification of Flavonols, Polyaromatic Amines and Their Metabolites in TI ww

The identification of kaempferol, quercetin, patuledin, rhamnetin, rhamnazin were performed from flavonols in the TI ww for the operational conditions given in the above section (Table 5a). In the MS spectrum; the m/z value of kaempferol was 464.2 after 25 min retention time with MS fragments of 412.1 and 445.3 at λ_{max} = 343 nm corresponding to [A+B+C+ D 2H$_3$O+ 3OH] with an benzenoid substituent. MS is an important tool for studying the interaction between small molecules and macromolecules. The bounds in benzene ring were cleaved

and the three -OH groups were separated by dehydroxylation from the kaempferol under UV irradiation. Kaempferol metabolites such as, 3-*O*-[2-*O*, 6-*O*-bis (*α*-L-rhamnosyl)-(*ß*-D-glucosyl] quercetin, 3-*O*-[6-*O*-(*α*-L -rhamnosyl)-(*ß*-D - glucosyl] quercetin, 3-*O*-{2-*O*-[6-*O*-(*p*-hydroxy-*trans*-cinnamoyl)-{) and *ß*-D -glucosyl]- *á*-L-rhamnosyl} were produced after 40 min irradiation time under 40 W/l UV-vis light power. The m/z ratios, the retention times, the λ$_{max}$ values and the MS spectrum of flavonol metabolites were given in Table 5a. These organics decreased with yields varying between 78% and 81% after 60 min UV-vis light irradiation time through mineralization of the metabolites to CO_2 and H_2O via photooxidation and photodegradation (Table 6a).

The MS spectrum of quercetin exhibited an ion peak at m/z 691.7 and it is assumed that to correspond to [B+A+3 benzene group +2H_2O] after 40 min irradiation time with at 40 W/l UV power (Table 5a). The quercetin with three benzenoid groups was cleaved to 3-*O*-[6-*O*-(*α*-L -rhamnosyl)-)-(*ß*-D-glucosyl] quercetin, 3-*O*-{2-*O*-[6-*O*-(*p*-hydroxy-*trans*-cinnamoyl)-(*ß*-D -glucosyl]-- *á*-L-rhamnosyl} as quercetin metabolites with m/z values of 234.4, 198.2 and 102.1, respectively, with 18 min, 19 and 21 min retention time, respectively (Table 5a). The quercetin metabolites decreased with high yields (85-86%) after 60 min of photooxidation and mineralized to CO_2 and H_2O (Table 6a).

Table 5a: Identification of flavonols and their metabolites in TI ww at La-ZnO NCs=30 mg/l with a La ratio of 1.5wt%, pH=8.0, after 60 min photooxidation time, at 50 W/l UV power and at 25ºC, respectively

RT (min)	UV (λ$_{max}$) (nm)	[M-H]⁻ (m/z)	MS fragments (ESI)	Identification
center				**Identification of flavonols and their metabolites in TI ww**
25	343	464.2	412.1	**Kaempferol**
3.29	313	345	408.1	3-*O*-[2-*O*,6-*O*-Bis(α-L-rhamnosyl)]-β-D--glucosyl]kaempferol
4.67	300	303	215.2	3-*O*-[2-*O*, 6-*O*-bis (¬-l-rhamnosyl)-(3-d-glucosyl] kaempferol
5.89	302	297	219.1	3-*O*-[6-*O*-(¬-l-rhamnosyl)-(3-d-glucosyl] kaempferol
23	313	691.7	598.08	**Quercetin**
18	298	234.4	212.3	3-*O*-[2-*O*, 6-*O*-bis (¬-l-rhamnosyl)-(3-d-glucosyl] quercetin
19	296	198.2	176.9	3-*O*-{2-*O*-[6-*O*-(*p*-hydroxy-*trans*-cinnamoyl)-(*ß*-D -glucosyl]-- *á*-L- rhamnosyl} quercetin
15	323	349.8	312.09	**Patuledin**
14	310	305.06	300.7	(E)-ascladiol
16	312	312.09	310.09	(Z)-ascladiol
15	310	398.07	389	**Rhamnetin**
14	299	234.45	289	Methyl quercetin
12	278	205.09	279	Tetrahydroxy-7-methoxyflavone
24.3	301	198.13	197.12	**Rhamnazin**
15	276	123.98	111.78	Rham nazin-3-0-ß-D -glucopyranosyl-(l →5)- α-L-arabinofuranoside
12	254	104.12	10.56	Rhamnazin-3-O-ß-D- glucopyranosyl-(l—»5)-[ß-D-apiofuranosyl-(-1→2)]-α -L-arabinofuranoside

Table 5b: Identification of polyaromatic amines and their metabolites in TI ww at La-ZnO NCs= 30 mg/l, with a La ratio of 1.5wt%, pH=8.0, after 60 min photooxidation time, at 50 W/l UV power and at 25ºC, respectively

RT (min)	UV (λ$_{max}$) (nm)	[M-H]⁻ (m/z)	MS fragments (ESI)	Identification
center				**Identification of polyaromatic amines and their metabolites in TI ww**
18	323	458	400	**2-methoxy-5-methylaniline**
20	309	216	209	5-nitro-o-toluidine
25	323	483.2	406.1	**2,4-diaminoanisole**
15	305	123.4	112.8	4-acetylamino-2-aminoanisole
18	302	116.5	110.3	2,4-diacetylaminoanisole
18.9	324	213.8	210.8	**4,40-diamino diphenyl ether**
15	320	189.6	170.7	N,N*l*-diacetyl-4,4*l*-diaminobenzhydrol
12	307	165.9	160.7	N,N*l*-diacetyl-4,4¹-diaminophenylmethane
27	342	595.1		**o-aminoazotoluene**
21	301	234.98		hydroxy-OAT (I)
19	298	222.07		4′ -hydroxy-OAAT
16	239	201.87		2′ -hydroxymethyl-3-methyl-4-aminoazobenzene
17	235	198.67		4, 4′-bis(otolylazo)-2, 2′ -dimethylazoxybenzene
24	343	459.45		**4-aminoazobenzol**
13	278	201.65		Phenylhydroxylamine
9	260	202	198.2	Nitrosobenzol

Table 6a: The metabolites of flavonols in the TI ww and removal efficiencies after 60 min irradiation time, at La-ZnO NCs=30 mg/l with a La ratio of 1.5wt% during photooxidation process at 50 W/l UV power, at pH=8.0 and at 25ºC, respectively

Flavonoids	Flavonoids metabolites	Influent concentrations (mg/l)	Effluent Concentrations (mg/l)	Removal efficiencies (%)
Kaempferol	3-*O*-[2-*O*, 6-*O*-bis (¬-l- rhamnosyl)-(3-d-glucosyl] kaempferol	5.7	0.86	86
	3-*O*-[2-*O*, 6-*O*-bis (¬-l- rhamnosyl)-(3-d-glucosyl] kaempferol	3.6	0.08	81
	3-*O*-{2-*O*-[6-*O*-(*p*-hydroxy-*trans*-cinnamoyl)-{)-, *β*-D - glucosyl]- *á*-L- rhamnosyl} kaempferol	4.7	0.95	78
Quercetin	3-*O*-[6-*O*-(*α*-L -rhamnosyl)-)-(*β*-D-glucosyl] quercetin	9.2	1.28	86
	3-*O*-{2-*O*-[6-*O*-(*p*-hydroxy-*trans*-cinnamoyl)-(*β*-D - glucosyl]-- *á*-L- rhamnosyl} quercetin	7.4	1.30	85
Patuledin	(E)-ascladiol	10.3	1.55	85
	(Z)-ascladiol	8.1	0.85	88
Rhamnetin	Methyl quercetin	7.2	1.15	84
	Tetrahydroxy-7-methoxyflavone	4.6	0.44	86
Rhamnazin	Rham nazin-3-0-ß-D -glucopyranosyl-(l →5)- *α*-L-arabinofuranoside	6.15	1.42	87
	Rhamnazin-3-O-ß-D- glucopyranosyl-(l—»5)-[ß-D-apiofuranosyl-(-1→2)]-*α* -L-arabinofuranoside	5.15	1.05	89

Table 6b: The metabolites of polyaromatic amines in the TI ww and removal efficiencies after 60 min irradiation time, at La-ZnO NCs=30 mg/l with a La ratio of 1.5wt% during photooxidation process, at 50 W/l UV irradiation, at pH=8.0 and at 25ºC, respectively

Polyaromatic amines	Polyaromatic amines metabolites	Influent concentrations (mg/l)	Effluent Concentrations (mg/l)	Removal efficiencies (%)
2-methoxy-5-methylaniline	5-nitro-o-toluidine	134.6	36.34	87
2,4-diaminoanisole	4-acetylamino-2-aminoanisole	275.8	22.06	92
	2,4-diacetylaminoanisole	200,5	38.61	90
4,40-diamino diphenyl ether	N,N*l*-diacetyl-4,4*l*-diaminobenzhydrol	156	28.08	82
	N,N*l*-diacetyl-4,4 *l* -diaminophenylmethane	116	40.56	84
o-aminoazotoluene	hydroxy-OAT (I)	293.6	58.72	80
	4′ -hydroxy-OAAT	200	79.27	83
	2′ -hydroxymethyl-3-methyl-4-aminoazobenzene	193.6	85.14	84
	4, 4′-bis(otolylazo)-2, 2′ -dimethylazoxybenzene	203.6	117.44	67
4-aminoazobenzol	Phenylhydroxylamine	158	39.16	78
	Nitrosobenzol	108	34.5	75

The m/z values of patuledin was 349.8 after 15 min retention time at a λmax of 323 nm corresponding to [A+B+ 2 benzene+ OH] after 40 min irradiation time. After 60 min UV irradiation time patuledin with two benzenoid rings were cleaved to A and to B metabolites via hydroxylation (Table 5a). At retention times of 24 mins and 19 mins, (E)-ascladiol and (Z)-ascladiol exhibited two [M + H]+ ion at m/z 305.06 and 312.09, respectively, which are compared with the theory molecular weight of (E)-ascladiol and (Z)-ascladiol and their fragmentations showed that they are consistent with the fragmentation of patuledin. Therefore, the compounds were assigned as (E)-ascladiol and (Z)-ascladiol. The Patuledin metabolites such as, (E)-ascladiol, (Z)-ascladiol removed with high yields (85-88%) after 60 min photooxıdation time (Table 6a).

Rhamnetin exhibited an ion peak at m/z 398.06, likely corresponding to [B+A+4 OH+CH] after 15 min retention time at λmax = 310 nm (Table 5a). The names of B and A metabolites were, methyl quercetin and tetrahydroxy-7-methoxyflavone with dehydroxylation of –OH and demethylation of –CH3 groups after cleaving of three

benzen rings, after 40 min irradiation with m/z values of 234.5 and 205.09, respectively (Table 5a). They were mineralized with high yields (84-86%) under 50 W/l UV-vis power, at 25ºC after 60 min photooxidation (Table 6a).

The last flavonol with a retention time of 24.3 min exhibited a [M + H]+ion at m/z 198.13 and its fragmentation by MS experiments showed that it was consistent with Rhamnazin and correspond to three –OH and 2 methyl groups with three benzene rings. After 40 min irradiation (Table 5a). The metabolites of Rhamnazine were Rhamnazin-3-0-ß-D - glucopyranosyl-(l →5)- α-L-arabinofuranoside and Rhamnazin-3-O-ß-D-glucopyranosyl-(l—»5)-[ß-D-apiofuranosyl-(-1→2)]-α-L-arabinofuranoside produced with dealkylation of two methyl group, dehydroxylation of three –OH groups and cleavege of 3 benzoic ring after 15 and 12 min retention times with m/z values of 123.98 and 104.12, respectively (Table 5a). Their removal yields varied between 87 and 89%, after 60 min photooxidation time, at 50 W/l UV-vis power and at 25ºC by mineralization process (Table 6a). The identification of Polyaromatic amines namely, 2-methoxy-5-methylaniline, 2,4-diaminoanisole,

4,40-diamino diphenyl ether, o-aminoazotoluene, 4-aminoazobenzol from TW were performed (Table 5b). In the MS spectrum, 2-methoxy-5-methylaniline exhibited an ion peak at m/z 458, assumed to correspond to [B+2CH₃+ NH₂+benzenoid ring] after 18 min retention time. By deamination, dealkylation and cleaving of double azo bonds 2-methoxy-5-methylaniline photodegraded to it's metabolite. 5-nitro-o-toluidine as the metabolite of 2-methoxy-5-methylaniline was produced after 40 min UV irradiation with m/z value of 216 (Table 5b). The yield of this metabolite was recorded as 87 % after 60 min photooxidation time, at 50 W/l UV-vis power via mineralization to CO_2 and H_2O (Table 6a).

The m/z values of aromatic amine namely, 2,4-diaminoanisole was 483.2 after 25 min retention times, at λ_{max} = 323 nm, respectively, corresponding to [A+B+ NH₂+ 3OH] and [A+B+ NH₂+ 2PHE+(C₂H₅)-2O] with an benzenoid ring (Table 5b). The metabolites of 2,4 diaminoanisole were 4-acetylamino-2-aminoanisole and 4,4-0-diamino diphenyl ether with m/z values of 123.4 and 116.5 produced by deamination and dephenilation and dealkylation processes after UV irradiation after 40 min of irradiation time (Table 5b). The photodegradation yields of thses metabolites were 90% and 92%, after 60 min irradiation time (Table 6b).

The third poly aromatic amine with a retention time of 18.9 min exhibited a [M + H]+ion at m/z 213.8 and its fragmentation by MS experiments showed that it was consistent with 4,40-diamino diphenyl ether and correspond to two amino, 2 dyphenyl and an ether radical groups with two benzenoid rings (Table 5b). The metabolites of 4,40-diamino diphenyl ether were N,Nⁱ-diacetyl-4,4ⁱ-diaminobenzhydrol and N,Nⁱ-diacetyl-4,4 ⁱ – diaminophenylmethane by dealkylation of two methyl and dehydroxylatın of three –OH groups and cleavege of 3 benzoic ring after 15 and 12 min retention times, respectively after 40 min of UV irradiation time (Table 5b). The photodegradation yields of the 4,40-diamino diphenyl ether metabolites varied between 82% and 84% (Table 6b). The MS spectrums of o-aminoazotoluene and 4-aminoazobenzol exhibited ion peaks at m/z 595.1 and 459.45 and they are assumed that to correspond to [B+A+ 1 azo -N =N, +1 amino + 2 methyl +2 benzene group] and to [A+B+C+D + 1 azo -N =N, +1 amino +2 benzene group], respectıvely (Table 5b). o-aminoazotoluene transformed to metabolites namely hydroxy-OAT (I), 4′ -hydroxy-OAAT, 2′ -hydroxymethyl-3-methyl-4-aminoazobenzene and 2′ -hydroxymethyl-3-methyl-4-aminoazobenzene by deaminification, demetylation, dealkylation mechanisms and by cleaving of double band of azo groups after 40 min of UV-vis light irradiation. The related MS fragments, retention times and m/z values was illustrated in Table 5b. The yields of metabolides varied between 67% and 84% (Table 6b). The 4-aminoazobenzol were photodegraded to Phenylhydroxylamine and to Nitrosobenzol by deamination, dehydroxylatın and cleaving of double band in azo groups (Table 5b). Their yields were between 75% and 78% (Table 6b).

3.7 Effect of Increasing La Mass Ratios on 30 mg/l La-ZnO NCs for Photodegradation of TI ww Pollutants

We researched the effects of different La mass ratios (0.5wt%, 1wt%, 1.5wt% and 2wt%) in La-ZnO NCs=30 mg/l on the photooxidation yields of all pollutants in the TI ww during photooxidation experiments. Maximum COD_total, COD_inert, total flavonols, TAAs and color removal efficiencies were 99%, 92%, 91%, 98% and 99%, respectively, after 60 min photooxidation time, at pH=8.0, at 1.5wt% La mass ratio and at 25ºC, respectively (Table 7). Removal efficiencies increased as the La mass ratio in the La-ZnO NCs were increased from 0.5wt% to 1wt% and to 1.5wt%. Maximum removal efficiencies was measured at 1.5wt% La mass ratio in the NCs. The photocatalytic degradation efficiency of ZnO NPs increases with an increase in the La loading and shows a maximum activity at 1.5 wt%. Then decreases in photooxidation yield was observed on further La doping (to 2 wt%). The reason of this can be explained as follows: excessive amounts of dopants can retard the photocatalysis process, because excess amount of dopants deposited on the surface of ZnO increases the recombination rate of free electrons and energized holes, thus inhibiting the photodegradation process. Hence, further increase in La doping to 2wt% results in the decrease of photocatalytic degradation efficiency.

Table 7: Effect of increasing La mass ratios on the TI ww during photooxidation process after 60 min, at 50 W/l UV irradiation, at La-ZnO NCs = 30 mg/l, at pH=8.0 and at 25ºC, respectively

Parameters	Removal efficiencies (%)			
	La mass ratios (%)			
	0.5wt%	1wt%	1.5wt%	2wt%
COD_total	46	71	99	80
COD_inert	40	69	92	74
COD_dissolved	45	70	98	78
Color	57	76	99	81
Total flavonols	35	64	91	75
Flavonols				
Kaempferol	30	63	87	68
Quercetin	31	67	88	69
Patuledin	32	68	90	75
Rhamnetin	33	62	87	68
Rhamnazin	30	60	85	67
TAAs	53	81	98	77
Polyaromatics				
2-methoxy-5-methylaniline	50	72	93	69
2,4-diaminoanisole	49	77	95	75
4,40-diamino diphenyl ether	47	64	87	64
o-aminoazotoluene	44	71	84	70
4-aminoazobenzol	41	70	82	66

3.8 Effect of Increasing Photooxidation Time on the Photooxidation Yields of Pollutants in the TI ww

Six different photooxidation times (5 min, 15 min, 30 min, 60 min, 80 min and 100 min) was examined during photocatalytic oxidation of the pollutants in the TI ww. To determine the optimum photooxidation time for maximum removals these pollutant parameters in the TI ww. The maximum photocatalytic oxidation removals was observed at 60 min photooxidation time, at pH=8.0 using La-ZnO NCs=30 mg/l with a La mass ratio of 1.5wt% at a 50 W UV power, respectively (Table 8).

Table 8: Effect of increasing photooxidation time on the TI ww during photooxidation process, at 50 W/l UV irradiation, at pH=8.0, at La-ZnO NCs = 30 mg/l, 1.5 wt% La mass ratio and at 25°C, respectively

Parameters	Removal efficiencies (%)					
	5 min	15 min	30 min	60 min	80 min	100 min
COD_{total}	56	69	87	99	95	95
COD_{inert}	50	67	81	92	92	91
$COD_{dissolved}$	55	68	85	98	97	97
Color	67	74	88	99	96	90
Total flavonols	45	63	82	91	86	80
Flavonols						
Kaempferol	40	61	75	87	86	86
Quercetin	41	65	77	88	86	85
Patuledin	41	66	81	90	89	89
Rhamnetin	43	61	74	87	85	84
Rhamnazin	39	58	72	85	80	79
TAAs	63	78	84	98	94	93
Polyaromatics						
2-methoxy-5-methylaniline	60	71	86	93	93	92
2,4-diaminoanisole	59	75	82	95	94	93
4,40-diamino diphenyl ether	57	62	71	87	79	78
o-aminoazotoluene	55	69	78	84	82	80
4-aminoazobenzol	51	62	75	82	81	79

The removals of COD_{total}, COD_{inert}, total flavonols, total aromatic amines and color were found to increase linearly with increase in retention time from 5 min up to 80 min. A further increase in retention time to and 100 min lead to a decrease in yields of pollutant parameters. In other words the removal efficiencies of pollutant parameters (COD components, flavonols, polyaromatics, color) decreased for photooxidation time > 60 min since at long irradiation times since the surface energy of La-ZnO NCs decreases (Fox and Dulay, 1993). The photooxidation can form small molecules such as H_2O, carbonmonoxide (CO), CO_2 and benzene (C_6H_6) etc., after long irradiation; it will lead to the decrease of the polar groups and the O_2 content of pollutant surface. The dispersive component of surface energy, the density of polymer surface has great influence on dispersivity of pollutants in the TI ww. However, the rate of photodegradation of La-ZnO NCs blends increases with the increase of irradiation time, and is higher than that of photocrosslinking after long irradiation time, leading to the decrease of the density of the polymer surface and the dispersivity of COD, dyes and other pollutants to La-ZnO NCs (Korake *et al*., 2014) [18]. The photooxidation can form small molecules such as H_2O, CO, CO_2 and C_6H_6 etc., after long irradiation; it will lead to the decrease of the polar groups and the O_2 content of polymer surface, therefore the dispersivity decreaeses resulting in low photooxidation yields (Korake *et al*., 2014) [18]. Aromatic and phenolic metabolites which would adsorb strongly onto La–ZnO NCs surface and block significant part of photoreactive sites.

3.9 Effect of Increasing UV-vis Light Powers on the Yields of Pollutants in the TI ww
In this study, four UV-vis light powers were used (10 W, 30 W, 50 W and 100 W) to detect the optimum UV irradiation power for maximum photo-removal of the pollutant parameters in the TI ww using La-ZnO NCs=30 mg/l with a La mass ratio of 1.5%w. The maximum photocatalytic oxidation removals was observed at 50 W/l UV-vis light irradiation, at pH=8.0, after 30 min photooxidation time and

at 25°C, respectively (Table 9).

Table 9: Effect of increasing UV-vis light irradiations on the TI ww during photooxidation process after 60 min, at La-ZnO NCs=30 mg/l, at pH=8.0 and at 25°C, respectively

Parameters	Removal efficiencies (%)			
	UV-vis light irradiation (W/l)			
	10 W/l	30 W/l	50 W/l	100 W/l
COD_{total}	49	82	99	97
COD_{inert}	43	76	92	90
$COD_{dissolved}$	48	81	98	96
Color	60	83	99	99
Total flavonols	38	76	91	90
Flavonols				
Kaempferol	33	70	87	87
Quercetin	34	71	88	86
Patuledin	35	78	90	89
Rhamnetin	36	70	87	87
Rhamnazin	33	71	85	85
TAAs	56	79	98	96
Polyaromatics				
2-methoxy-5-methylaniline	53	81	93	92
2,4-diaminoanisole	52	77	95	93
4,40-diamino diphenyl ether	50	66	87	86
o-aminoazotoluene	47	73	84	81
4-aminoazobenzol	45	71	82	80

The COD_{total}, COD_{inert} total flavonols, TAAs and color were found to increase linearly with increase in UV-vis light irradiation from 10 W/l, up to 30 W/l, up to 50 W/l, respectively (Table 9). Further increase of UV-vis power up to 100 W did not affect positively the pollutant yields. Maximum COD_{total}, COD_{inert}, total flavonols, TAAs and color removal efficiencies after photooxidation process varied between 91% and 99% (Table 9). Flavonols such as kaempferol, quercetin, patuledin, rhamnetin, rhamnazin removal efficiencies were 87%, 88%, 90%, 87% and 85%, respectively, after 60 min photooxidation time, at 50 W/l UV light, at pH=8.0, at La-ZnO NCs= 30 mg/l and at 25°C, respectively (Table 9). Polyaromatic amines such as, 2-methoxy-5-methylaniline, 2, 4-diaminoanisole, 4, 40-diamino diphenyl ether, o-aminoazotoluene, 4-aminoazobenzol removal efficiencies after photooxidation process varıed between 82% and 93% (Table 9). The UV power determines the extent of light absorption by the semiconductor catalyst at a given wavelength. During initiation of photocatalysis, electron–hole formation in the photochemical reaction is strongly dependent on the optimum light intensity (Cassano and Alfano, 2000) [6]. In this study, as the UV-vis power increase from 10 W/l up to 50 W/l might favor a high-level surface defects, which account for the increase in the defect emission relative to the UV emission as reported by Selvam *et al*. (2013) [27]. Higher UV-vis powers > 50 W/l decrease the defects in the surface of the NPs by disturbing the active holes.

3.10 Effect of Increasing pH Values on the Pollutant Yields in the TI ww
The effects of increasing pH values (4.0, 6.0, 8.0 and 10.0) on the photocatalytic oxidation of polutant parameters in TI ww was examined by considering the solubility of ZnO NPs in acidic as well as in highly basic solutions. The maximum photocatalytic oxidation removals was obtained at pH=8.0, after 60 min photooxidation time with a La mass ratio 1.5wt% using La-ZnO NCs = 30 mg/l, at 50 W/l UV power

and at 25°C, respectively (Table 10).

Parameters	Removal efficiencies (%)			
	pH values			
	pH=4.0	pH=6.0	pH=8.0	pH=10.0
COD$_{total}$	53	74	99	72
COD$_{inert}$	47	72	92	70
COD$_{dissolved}$	52	73	98	71
Color	64	79	99	77
Total flavonols	42	68	91	66
Flavonols				
Kaempferol	37	66	87	64
Quercetin	38	70	88	68
Patuledin	39	71	90	69
Rhamnetin	40	66	87	64
Rhamnazin	45	62	85	60
TAAs	60	83	98	81
Polyaromatics				
2-methoxy-5-methylaniline	57	76	93	74
2,4-diaminoanisole	56	80	95	78
4,40-diamino diphenyl ether	54	67	87	65
o-aminoazotoluene	52	74	84	72
4-aminoazobenzol	50	65	82	63

In acidic medium, less photocatalytic degradation of pollutant parameters (COD components, flavonols, polyaromatics, color) was observed. The extent of photocatalytic degradation of polutant parameters was found to increase with increase in initial pH=8.0 and a decrease in maximum photocatalytic degradation was found at pH=10.0. The possible explanation of this is that the pH at zero point charge (ZPC) of ZnO is pH=9.0 ± 0.3 (Anandan *et al*., 2006) [1]. Below pH=8.0, active sites on the positively charged catalyst surface are preferentially covered by pollutant molecules. Thus, surface concentration of the polutant parameters (COD components, flavonols, polyaromatics, color) is relatively high, while those of OH$^-$ and OH$^\bullet$ are low. Hence, photocatalytic degradation decreases at acidic pH. On the other hand, above pH=8.0, catalyst surface is negatively charged by means of metal-bound OH$^-$, consequently the surface concentration of the polutant parameters (COD components, flavonols, polyaromatics, color) is low, and OH$^\bullet$ is high. In addition, polutant parameters are not protonated above pH=8.0. The electrostatic repulsion between the surface charges and La-ZnO NCs hinders the amount of polutant parameters and the adsorption, consequently surface concentration of the polutant parameters decreases, which results in the decrease of photocatalytic degradation at pH=10.0. In conclusion, pH=8.0 can provide moderate surface concentration of polutant parameters which react with the holes to form OH$^\bullet$.

3.11 Photocatalytic Oxidation Mechanisms of La-ZnO NCs

The higher activity of La-ZnO NCs can be attributed to successful e$^-$–h$^+$ separation and production of $^\bullet$O$_2^-$ and OH$^\bullet$. La-modified ZnO sample manifests the highest efficiency, related to the different charge and electronegativity of La and Zn ions and as a result of stronger adsorption of OH$^-$ions onto the ZnO surface (Anandan *et al*., 2007a) [2]. This favors the formation of OH$^\bullet$ by reaction of hole and OH$^-$. The OH$^\bullet$ and photogenerated $^\bullet$O$_2^-$ has extremely

strong non-selective oxidants lead to the degradation of the organic pollutant at the surface of La modified ZnO (Korake *et al*., 2014) [18]. The photocatalytic degradation mechanism starts with the illumination of ZnO NPs and production of electron–hole pairs in Equation (1):
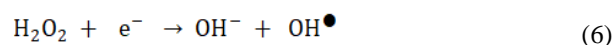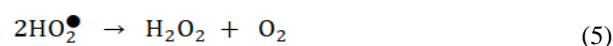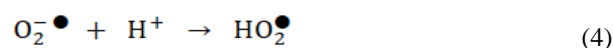
$$ZnO + h_v(UV) \rightarrow e^- + h^+ \tag{1}$$
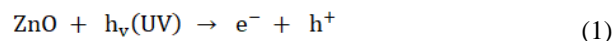
The ability of La^{+3} to scavenge photogenerated electrons is as follows: (Equation 2):

$$La^{+3} + e^- \rightarrow La^{+2} \tag{2}$$

However, stabilities of La^{+3} ions may be disturbed in their reduced forms (La^{+2}). This can be achieved by transferring the trapped electron to O$_2$ in Equation (3):
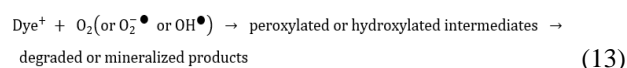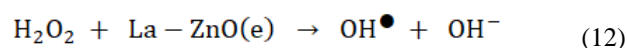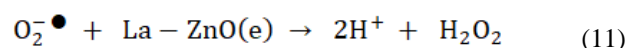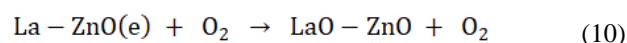
$$La^{+2} + O_2 \rightarrow La^{+3} + O_2^{-\bullet} \tag{3}$$
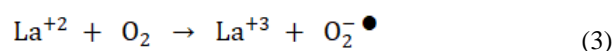
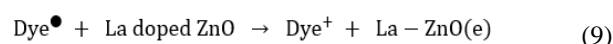The produced O$_2^{-\bullet}$ is responsible from the generation of OH$^\bullet$, known as highly reactive electrophilic oxidants (Equation 4, Equation 5 and Equation 6):

$$O_2^{-\bullet} + H^+ \rightarrow HO_2^\bullet \tag{4}$$

$$2HO_2^\bullet \rightarrow H_2O_2 + O_2 \tag{5}$$

$$H_2O_2 + e^- \rightarrow OH^- + OH^\bullet \tag{6}$$

In the meantime, photogenerated holes may react with H$_2$O molecules and produce OH$^\bullet$ (Equation 7):

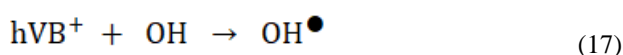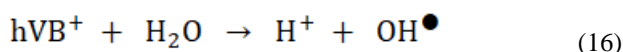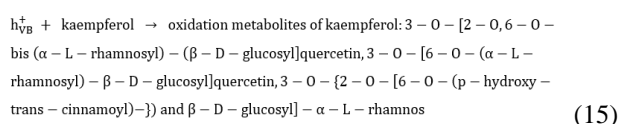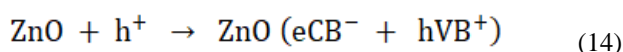$$h_{VB}^+ + H_2O \rightarrow H^+ + OH^\bullet \tag{7}$$
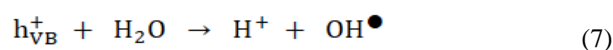
The color removal by photooxidation reactions of dyes in TW were given in Equation 8, Equation 9, Equation 10, Equation 11, Equation 12 and Equation13:
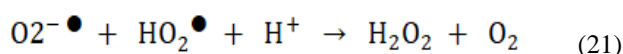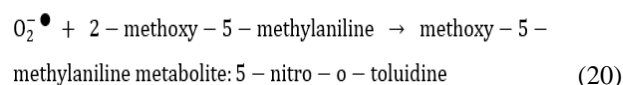
$$Dye + h_v \rightarrow Dye^\bullet \tag{8}$$

$$Dye^\bullet + La\,doped\,ZnO \rightarrow Dye^+ + La-ZnO(e) \tag{9}$$

$$La-ZnO(e) + O_2 \rightarrow LaO-ZnO + O_2 \tag{10}$$

$$O_2^{-\bullet} + La-ZnO(e) \rightarrow 2H^+ + H_2O_2 \tag{11}$$

$$H_2O_2 + La-ZnO(e) \rightarrow OH^\bullet + OH^- \tag{12}$$

$$Dye^+ + O_2(or\,O_2^{-\bullet}\,or\,OH^\bullet) \rightarrow peroxylated\,or\,hydroxylated\,intermediates \rightarrow degraded\,or\,mineralized\,products \tag{13}$$

For La–ZnO NCs, electron accepting ability, production of more OH$^\bullet$, the highest surface roughness value and the higher dark adsorption capacity result in pronounced photoactivity. The decay profile of the products includes the subsequent attacks of OH$^\bullet$, known as highly reactive electrophilic oxidants. The main reaction pathway is the addition of the OH$^\bullet$ to the double bond of the azo, methyl amino, benzenoid group, resulting in the rapid disappearance of color; flavonoid and aromatic amines

(Joseph *et al*., 2000) [15]. Further $OH^\bullet$ attacks and the increment in $OH^\bullet$ concentration in the solution increase the yield of OH-adduct in the degradation progress of each product. The opening of the dye aromatic rings due to consecutive oxidation reactions leads to low-molecular weight compounds (Galindo *et al*., 2000) [9].

Under the irradiation of lanthanides ions as an electron scavenger, the superoxide species prevent the holes–electrons (h^+/e^-) recombination, and thus increases photooxidation efficiency. Direct band gap excitation of the semiconductor results in electron–hole separation. The high oxidative potential of the hole (hVB^+) in the catalyst permits the direct oxidation of flavonols and aromatic amines to reactive intermediates. The $OH^\bullet$ and photo generated holes are extremely strong, that lead to photodegradation of the flavonols in the TI ww at the catalysts surface (Equation 14, Equation 15, Equation 16 and Equation 17):

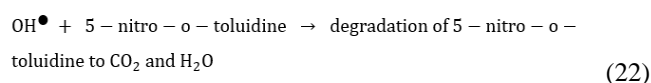$$ZnO + h^+ \rightarrow ZnO \, (eCB^- + hVB^+) \tag{14}$$

h_{VB}^+ + kaempferol → oxidation metabolites of kaempferol: $3 - O - [2 - O, 6 - O -$ bis $(\alpha - L - rhamnosyl) - (\beta - D - glucosyl]$quercetin, $3 - O - [6 - O - (\alpha - L -$ rhamnosyl$) - \beta - D - glucosyl]$quercetin, $3 - O - \{2 - O - [6 - O - (p - hydroxy -$ trans $-$ cinnamoyl$)-\}) $ and $\beta - D - glucosyl] - \alpha - L - rhamnos$ (15)

$$hVB^+ + H_2O \rightarrow H^+ + OH^\bullet \tag{16}$$

$$hVB^+ + OH \rightarrow OH^\bullet \tag{17}$$

Electron in the conduction band (eCB^-) on the catalyst surface can reduce molecular O_2 to superoxide anion (O_2^-) (Equation 18 and Equation 19). This radical, in the presence of organic scavengers such as polyaromatic amines, may form organic peroxides (Equation 20) or hydrogen peroxide (H_2O_2) (Equation 21):

$$La^{+3} + O_2 \rightarrow La^{+2} + O_2 \tag{18}$$

$$eCB^- \rightarrow O_2 \rightarrow O_2^{-\bullet} \tag{19}$$

$O_2^{-\bullet}$ + 2 − methoxy − 5 − methylaniline → methoxy − 5 − methylaniline metabolite: 5 − nitro − o − toluidine (20)

$$O2^{-\bullet} + HO_2^\bullet + H^+ \rightarrow H_2O_2 + O_2 \tag{21}$$
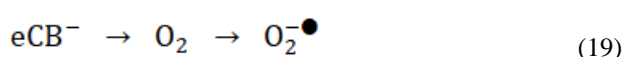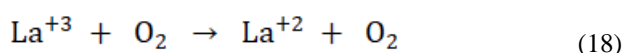
Electrons in the conduction band are also responsible for the production of $OH^\bullet$, which have been indicated as the primary cause of 2-methoxy-5-methylaniline mineralization which one of the polyaromatic amines in TI ww (Equation 22) (Selvam *et al*., 2013) [27]:

$OH^\bullet$ + 5 − nitro − o − toluidine → degradation of 5 − nitro − o − toluidine to CO_2 and H_2O (22)

3.12 Reusability of La-ZnO NCs
The reproducibility of the La-ZnO NCs=30 mg/l for flovonols and polyaromatic amines photodegradations were performed in a six-cycle experiment. As shown in Fig 9, after the first cycle of photocatalytic oxidation within 60 min, 99% of the La-ZnO NCs with a mass ratio of 1.5wt% was recovered. After each photo-degradation experiment, the NCs was separated from the TI ww and it was added new TI ww samples. After three cycles, the phoooxidation ability of La-ZnO NCs was retained at 98.9% of the original value. After 8th cycles the NCs was reatined at 98%. One of the reasons for the slight decline in photooxidation after 8th cycles is that the surface of the reused photocatalysts may exist with some low residual substances originated from organic substances, from flavonoid and polyaromatic substances which did not occupy the photocatalytic sites and did not block the adsorption. It is possible that the oxygen atom (O_2) in La-ZnO NCs was be sligtly bounded to the dopant La (Pala and Metiu, 2007) [23]. In our study, according to SEM and XRD analysis La_2O_3 was not observed. However, it can not be speculated from an corrosion problem since the size of NCs was not changed after photooxidation and remained as is before UV (λ_{max} = 310 nm). No photocorrosion of ZnO was observed due to the absence of $Zn(OH)_2$ since the corrosion products consist mainly of this component and La_2O_3 was not observed as separate phase. This indicated that the ZnO NPs was not dissociated and a photocorrosion problem was not observed.
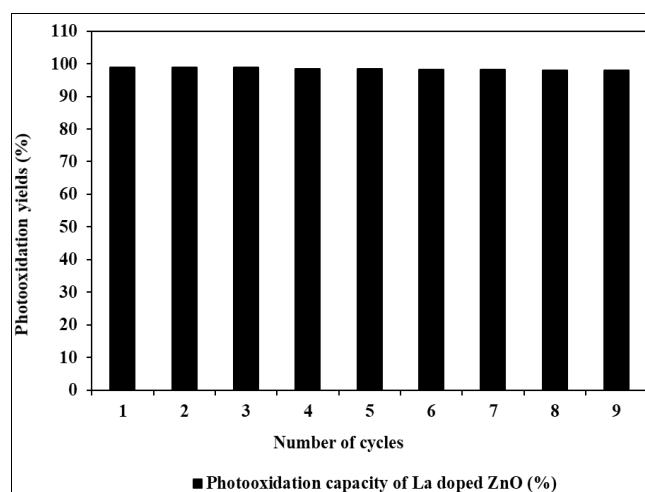
Fig 9: The reusability of La-ZnO NCs

3.13 Effect of La-ZnO NCs Concentrations on the Acute Toxicity Removal Efficiencies in TI ww at Increasing Sonication Time and Temperature
3.13.1 Effect of La-ZnO NCs Concentrations on the Microtox Acute Toxicity Removal Efficiencies in TI ww at Increasing Sonication Time and Temperature
In Microtox with *Aliivibrio fischeri* (also called *Vibrio fischeri*) acute toxicity test, the initial EC_{90} values at pH=7.0 was found as 825 mg/l at 25°C (Table 11: SET 1). After 60 min, 120 and 150 min of photooxidation time the EC_{90} values decreased to EC_{55}=414 mg/l to EC_{20}=236 mg/l and to EC_{10}=165 mg/l in La-ZnO NCs=10 mg/l at 30°C (Table 11: SET 3). The Microtox acute toxicity removal efficiencies were 38.89%, 77.78% and 88.89% after 60 min, 120 and 150 min photooxidation time, respectively, in La-ZnO NCs=10 mg/l and at 30°C (Table 11: SET 3).

Table 11: Effect of increasing La-ZnO NCs concentrations on Microtox acute toxicity in TI ww, at 50 W/l UV-vis power, at 30ºC and at 60ºC, respectively

S. No	Parameters	Microtox Acute Toxicity Values, * EC (mg/l)							
		25ºC							
		0. min		60. min		120. min		150. min	
		*EC$_{90}$		*EC		*EC		*EC	
1	Raw ww, control	825		EC$_{70}$=510		EC$_{60}$=650		EC$_{50}$=640	
		30ºC				60ºC			
		0. min	60. min	120. min	150. min	0. min	60. min	120. min	150. min
		*EC$_{90}$	*EC	*EC	*EC	*EC$_{90}$	*EC	*EC	*EC
2	Raw ww, control	825	EC$_{70}$= 580	EC$_{50}$= 580	EC$_{40}$= 550	825	EC$_{55}$=550	EC$_{40}$= 590	EC$_{30}$= 690
3	La-ZnO NCs=0.10 mg/l	825	EC$_{60}$= 422	EC$_{25}$= 241	EC$_{15}$= 168	825	EC$_{55}$= 419	EC$_{20}$= 266	EC$_{10}$= 150
	La-ZnO NCs=0.50 mg/l	825	EC$_{60}$= 421	EC$_{25}$= 239	EC$_{15}$= 167	825	EC$_{55}$= 414	EC$_{20}$= 232	EC$_{10}$= 161
	La-ZnO NCs=10 mg/l	825	EC$_{55}$ =414	EC$_{20}$= 236	EC$_{10}$= 165	825	EC$_{50}$= 550	EC$_{15}$= 540	EC$_{5}$= 500
	La-ZnO NCs=20 mg/l	825	EC$_{65}$= 408	EC$_{30}$= 230	EC$_{20}$= 162	825	EC$_{60}$= 403	EC$_{25}$= 218	EC$_{15}$= 148
	* EC values were calculated based on COD$_{dis}$ (mg/l).								

The EC$_{90}$ values decreased to EC$_{50}$, to EC$_{15}$ and to EC$_{5}$ after 60 min, 120 and 150 min photooxidation times, respectively, in La-ZnO NCs=10 mg/l at 60ºC (Table 11: SET 3). The EC$_{50}$, the EC$_{15}$ and the EC$_{5}$ values were measured as 550 mg/l, 540 and 500 mg/l, respectively, in La-ZnO NCs=10 mg/l at 60ºC. The toxicity removal efficiencies were 44.44%, 83.33% and 94.44% after 60 min, 120 and 150 min photooxidation time, respectively, in La-ZnO NCs=10 mg/l at 60ºC (Table 11: SET 3). 94.44% maximum Microtox acute toxicity removal yield was found in La-ZnO NCs=10 mg/l after 150 min photooxidation time and at 60ºC (Table 11: SET 3).

The EC$_{90}$ values decreased to EC$_{60}$=422 mg/l to EC$_{25}$=241 and to EC$_{15}$=168 mg/l after 60 min, 120 and 150 min photooxidation times, respectively, in La-ZnO NCs=0.10 mg/l at 30ºC (Table 11: SET 3). The EC$_{90}$ values decreased to EC$_{60}$=421 mg/l to EC$_{25}$=239 and to EC$_{15}$=167 mg/l after 60 min, 120 and 150 min photooxidation times, respectively, in La-ZnO NCs=0.50 mg/l at 30ºC. The EC$_{90}$ values decreased to EC$_{65}$=408 mg/l to EC$_{30}$=230 and to EC$_{20}$=162 mg/l after 60 min, 120 and 150 min photooxidation times, respectively, in La-ZnO NCs=20 mg/l at 30ºC. The Microtox acute toxicity removals were 83.33%, 83.33% and 77.78% in 0.10, 0.50 and 20 mg/l La-ZnO NCs, respectively, after 150 min photooxidation time at 30ºC. It was obtained an inhibition effect of La-ZnO NCs=20 mg/l to *Vibrio Fischeri* after 150 min photooxidation time and at 30ºC (Table 11: SET 3).

The EC$_{90}$ values decreased to EC$_{55}$=419 mg/l to EC$_{20}$=266 and to EC$_{10}$=150 mg/l after 60 min, 120 and 150 min photooxidation times, respectively, in La-ZnO NCs=0.10 mg/l at 60ºC (Table 11: SET 3). The EC$_{90}$ values decreased to EC$_{55}$=414 mg/l to EC$_{20}$=232 and to EC$_{10}$=161 mg/l after 60 min, 120 and 150 min photooxidation times, respectively, in La-ZnO NCs=0.50 mg/l at 60ºC. The EC$_{90}$ values decreased to EC$_{60}$=403 mg/l to EC$_{25}$=218 and to EC$_{15}$=148 mg/l after 60 min, 120 and 150 min photooxidation times, respectively, in La-ZnO NCs=20 mg/l at 60ºC. The Microtox acute toxicity removals were 88.89%, 88.89% and 83.33% in 0.10, 0.50 and 20 mg/l La-ZnO NCs, respectively, after 150 min photooxidation time at 60ºC. It was observed an inhibition effect of La-ZnO NCs=20 mg/l to Microtox with *Vibrio Fischeri* after 150 min photooxidation time and at 60ºC (Table 11: SET 3).

3.13.2 Effect of La-ZnO NCs Concentrations on the *Daphnia magna* Acute Toxicity Removal Efficiencies in TI ww at Increasing Sonication Time and Temperature

The initial EC$_{50}$ values were observed as 850 mg/l at 25ºC (Table 12: SET 1). After 60 min, 120 and 150 min of photooxidation time the EC$_{50}$ values decreased to EC$_{30}$=350 mg/l to EC$_{15}$=240 mg/l and to EC$_{10}$=90 mg/l in La-ZnO NCs=10 mg/l, at 30ºC (Table 12: SET 3). The toxicity removal efficiencies were 40%, 70% and 80% after 60 min, 120 and 150 min photooxidation times, respectively, in La-ZnO NCs=10 mg/l at 30ºC (Table 12: SET 3).

Table 12: Effect of increasing La-ZnO NCs concentrations on *Daphnia magna* acute toxicity in TI ww at 30ºC and at 60ºC (50 W/l UV-vis power)

S. No	Parameters	*Daphnia magna* Acute Toxicity Values, * EC (mg/l)							
		25ºC							
		0. min		60. min		120. min		150. min	
		*EC$_{50}$		*EC		*EC		*EC	
1	Raw ww, control	850		EC$_{45}$=625		EC$_{40}$=370		EC$_{30}$=155	
		30ºC				60ºC			
		0. min	60. min	120. min	150. min	0. min	60. min	120. min	150. min
		*EC$_{50}$	*EC	*EC	*EC	*EC$_{50}$	*EC	*EC	*EC
2	Raw ww, control	850	EC$_{40}$= 470	EC$_{35}$= 230	EC$_{25}$= 115	850	EC$_{35}$= 375	EC$_{30}$= 212	EC$_{20}$= 75
3	La-ZnO NCs=0.10 mg/l	850	EC$_{35}$= 450	EC$_{20}$= 145	EC$_{15}$= 260	850	EC$_{30}$= 130	EC$_{15}$= 425	EC$_{10}$= 340
	La-ZnO NCs=0.50 mg/l	850	EC$_{35}$= 450	EC$_{20}$= 175	EC$_{15}$= 100	850	EC$_{30}$= 425	EC$_{15}$= 140	EC$_{5}$= 90
	La-ZnO NCs=10 mg/l	850	EC$_{30}$= 350	EC$_{15}$= 240	EC$_{10}$= 90	850	EC$_{25}$= 150	EC$_{10}$= 60	EC$_{5}$= 375
	La-ZnO NCs=20 mg/l	850	EC$_{40}$= 300	EC$_{25}$= 170	EC$_{20}$= 52	850	EC$_{35}$= 250	EC$_{20}$= 110	EC$_{15}$= 11
	* EC values were calculated based on COD$_{dis}$ (mg/l).								

The EC_{50} values decreased to EC_{25} to EC_{10} and to EC_5 after 60 min, 120 and 150 min photooxidation times, respectively, in La-ZnO NCs=10 mg/l at 60ºC (Table 12: SET 3). The EC_{25}, the EC_{10} and the EC_5 values were measured as 150 mg/l, 60 and 375 mg/l, respectively, in La-ZnO NCs=10 mg/l at 60ºC. The toxicity removal efficiencies were 50%, 80% and 90% after 60 min, 120 and 150 min photooxidation times, respectively, in La-ZnO NCs=10 mg/l at 60ºC (Table 12: SET 3). 90% maximum *Daphnia magna* acute toxicity removal was obtained in La-ZnO NCs=10 mg/l after 150 min photooxidation time and at 60ºC, respectively (Table 12: SET 3).

The EC_{50} values decreased to EC_{35}=450 mg/l to EC_{20}=145 and to EC_{15}=260 mg/l after 60 min, 120 and 150 min photooxidation times, respectively, in La-ZnO NCs=0.10 mg/l at 30ºC (Table 12: SET 3). The EC_{50} values decreased to EC_{35}=450 mg/l to EC_{20}=175 and to EC_{15}=100 mg/l after 60 min, 120 and 150 min photooxidation times, respectively, in La-ZnO NCs=0.50 mg/l and at 30ºC. The EC_{50} values decreased to EC_{40}=300 mg/l to EC_{25}=170 and to EC_{20}=52 mg/l after 60 min, 120 and 150 min photooxidation times, respectively, in La-ZnO NCs=20 mg/l and at 30ºC. The *Daphnia magna* acute toxicity removals were 70%, 70% and 60% in 0.10, 0.50 and 20 mg/l La-ZnO NCs, respectively, after 150 min photooxidation time and at 30ºC. It was observed an inhibition effect of La-ZnO NCs=20 mg/l to *Daphnia magna* after 150 min photooxidation time and at 30ºC (Table 12: SET 3).

The EC_{50} values decreased to EC_{30}=130 mg/l to EC_{15}=425 and to EC_{10}=340 mg/l after 60 min, 120 and 150 min photooxidation times, respectively, in La-ZnO NCs=0.10 mg/l and at 60ºC (Table 12: SET 3). The EC_{50} values decreased to EC_{30}=425 mg/l to EC_{15}=140 and to EC_5=90 mg/l after 60 min, 120 and 150 min photooxidation times, respectively, in La-ZnO NCs=0.50 mg/l and at 60ºC. The

EC_{50} values decreased to EC_{35}=250 mg/l to EC_{20}=110 and to EC_{15}=11 mg/l after 60 min, 120 and 150 min photooxidation times, respectively, in La-ZnO NCs=20 mg/l and at 60ºC. The *Daphnia magna* acute toxicity removals were 80%, 90% and 70% in 0.10, 0.50 and 20 mg/l La-ZnO NCs, respectively, after 150 min photooxidation time and at 60ºC. It was observed an inhibition effect of La-ZnO NCs=20 mg/l to *Daphnia magna* after 150 min photooxidation time and at 60ºC (Table 12: SET 3).

Increasing the La-ZnO NCs concentrations from 0.10 to 20 mg/l did not have a positive effect on the decrease of EC_{50} values as shown in Table 12 at SET 3. La-ZnO NCs concentrations > 10 mg/l decreased the acute toxicity removals by hindering the photooxidation process. Similarly, a significant contribution of increasing La-ZnO NCs concentration to acute toxicity removal at 60ºC after 150 min of photooxidation time was not observed. Low toxicity removals found at high La-ZnO NCs concentrations could be attributed to their detrimental effect on the *Daphnia magna* (Table 12: SET 3).

3.13.3 Direct Effects of La-ZnO NCs Concentrations on the Acute Toxicity of Microtox and *Daphnia magna* in TI ww

The acute toxicity test was performed in the samples containing 0.10 mg/l, 0.50 mg/l, 10 mg/l and 20 mg/l La-ZnO NCs concentrations. In order to detect the direct responses of Microtox and *Daphnia magna* to the increasing La-ZnO NCs concentrations the toxicity test were performed without TI ww. The initial EC values and the the EC_{50} values were measured in the samples containing increasing La-ZnO NCs concentrations after 150 min photooxidation time. Table 13 showed the responses of Microtox and *Daphnia magna* to increasing La-ZnO NCs concentrations.

Table 13: The responses of Microtox and *Daphnia magna* acute toxicity tests in addition of increasing La-ZnO NCs concentrations without TI ww after 150 min photooxidation time

La-ZnO NCs Conc. (mg/l)	Microtox Acute Toxicity Test			*Daphnia magna* Acute Toxicity Test		
	Initial Acute Toxicity EC_{50} Value (mg/l)	Inhibitions after 150 min Photooxidation	EC Values (mg/l)	Initial Acute Toxicity EC_{50} Value (mg/l)	Inhibitions after 150 min Photooxidation	EC Values (mg/l)
0.10	EC_{10}= 25	-	-	EC_{10}= 40	-	-
0.50	EC_{15}= 80	4.00	EC_1= 4.00	EC_{20}= 100	6.00	EC_3= 6.00
10	EC_{20}= 150	6.00	EC_4= 7.00	EC_{30}= 200	7.00	EC_6= 12.00
20	EC_{25}= 220	8.00	EC_6= 10.00	EC_{40}= 300	10.00	EC_8= 16.00

The acute toxicity originating only from 0.10 mg/l, 0.50 mg/l, 10 mg/l and 20 mg/l La-ZnO NCs were found to be low (Table 13). 0.10 mg/l La-ZnO NCs did not exhibited toxicity to *Vibrio Fischeri* and *Daphnia magna* before and after 150 min photooxidation time. The toxicity atributed to the 0.50 mg/l, 10 mg/l and 20 mg/l La-ZnO NCs were found to be low in the samples without TI ww for the test organisms mentioned above. The acute toxicity originated from the La-ZnO NCs decreased significantly to EC_1, EC_4 and EC_6 after 150 min photooxidation time. Therefore, it can be concluded that the toxicity originating from the La-ZnO NCs is not significant and the real acute toxicity throughout photooxidation was attributed to the TI ww, to their metabolites and to the photodegradation by-products (Table 13).

4. Conclusions
By using 30 mg/l La-ZnO NCs with a La mass ratio of

1.5wt% the COD_{total}, COD_{inert}, flavonols, polyaromatics and color in TI ww were photodegraded with yields as high as 82-99% within 60 min photooxidation time, at 25ºC under 50 W/l UV power and at pH=8.0, respectively. The flavonoids and polyaromatic amines and their metabolites in the TI ww were determined and photodegraded with high photocatalysis rates (74%-95%) using 30 mg/l La-ZnO NCs. It is concluded that the TI ww can be treated by La-ZnO NCs under optimized operational conditions.

94.44% maximum Microtox acute toxicity yield was found in La-ZnO NCs=10 mg/l after 150 min photooxidation time and at 60ºC, respectively. It was observed an inhibition effect of La-ZnO NCs=20 mg/l to Microtox with *Vibrio Fischeri* after 150 min photooxidation time at 60ºC. 90% maximum *Daphnia magna* acute toxicity removal was obtained in La-ZnO NCs=10 mg/l after 150 min photooxidation time and at 60ºC, respectively. It was observed an inhibition effect of La-ZnO NCs=20 mg/l to

Daphnia magna after 150 min photooxidation time and at 60°C. La-ZnO NCs concentrations > 10 mg/l decreased the acute toxicity removals by hindering the photooxidation process. Similarly, a significant contribution of increasing La-ZnO NCs concentrations to acute toxicity removal at 60°C after 150 min of photooxidation time was not observed. Finally, it can be concluded that the toxicity originating from the La-ZnO NCs is not significant and the real acute toxicity throughout photooxidation was attributed to the TI ww, to their metabolites and to the photodegradation by-products.

5. Acknowledgements

6. References

1. Anandan S, Vinu A, Venkatachalam N, Arabindoo B, Murugesan V. Photocatalytic activity of ZnO impregnated Hâ and mechanical mix of ZnO/Hâ in the degradation of monocrotophos in aqueous solution. J. Mol. Catal. A: Chem. 2006; 256:312-320.
2. Anandan S, Vinu A, Mori T, Gokulakrishnan N, Srinivasu P, Murugesan V, *et al*. Photocatalytic degradation of 2,4,6-trichlorophenol using lanthanum doped ZnO in aqueous suspension. Cataly. Com. 2007a; 8:1377-1382.
3. Anandan S, Vinu A, Sheeja Lovely KLP, Gokulakrishnan N, Srinivasu P, Mori T, *et al*. Photocatalytic activity of La-doped ZnO for the degradation of monocrotophos in aqueous suspension. J. Mol. Catal. A: Chem. 2007b; 266:149-157.
4. Baird RB, Eaton AD and Rice EW, Rice EW (editors). Standard Methods for the Examination of Water and Wastewater. (23rd. Ed.). American Public Health Association (APHA), American Water Works Association (AWWA), Water Environment Federation (WEF). American Public Health Association 800 I Street, NW Washington DC: 20001-3770, USA, January 1, 2017. ISBN-13:978-0875532875, ISBN-10:087553287X
5. Byrappa K, Subramania AK, Ananda S, Rai KML, Dinesh R, Yushimura M. Photocatalytic degradation of Rhodamine B dye by ZnO. Bull. Mater. Sci. 2006; 29(5):433-438.
6. Cassano AE, Alfano OM. Reaction engineering of suspended solid heterogenous photocatalytic reactors. Catal. Today. 2000; 58:167-197.
7. Chung KT, Stevens SEJ. Degradation of azo dyes by environmental microorganisms and helminthes. Environ. Toxicol. Chem. 1993; 12:2121-2132.
8. Fox MA, Dulay MT. Hetereogeneous photocatalysis. Chem. Rev. 1993; 93:341-357.
9. Galindo C, Jacques P, Kalt A. Photodegradation of the aminobenzene Acid Orange 52 by three advanced oxidation processes: UV/H_2O_2, UV/TiO_2 and VIS/TiO_2: comparative mechanistic and kinetic investigations. J. Photochem. Photobiol. A. 2000; 130:35-47.
10. Ganesh I, Sekhar PSC, Padmanabham G, Sundararajan G. Influence of Li-doping on structural characteristics and photocatalytic activity of ZnO nano-powder formed in a novel solution pyro-hydrolysis route. Appl. Surf. Sci. 2012; 259:524-537.
11. Germirli F, Orhon D, Artan N. Assessment of the initial inert soluble COD in industrial wastewater. Water. Sci. Technol. 1991; 23:1077-1086.
12. Gouvea K, Wypych F, Moraes SG, Duran N, Nagata N, Peralta-Zamora P. Semiconductor-Assisted photocatalytic degradation of reactive dyes in aqueous solution. Chemosphere. 2000; 40:433-440.
13. Huang M, Xu C, Wu Z, Huang Y, Lin J, Wu J. Photocatalytic discolorization of Methyl Orange solution by Pt modified TiO_2 loaded on natural zeolite. Dyes Pigments. 2008; 77:327-334.
14. Jia T, Wang W, Long F, Fu Z, Wang H, Zhang Q. Fabrication, characterization and photocatalytic activity of La-doped ZnO nanowires. J. Alloys Compd. 2009; 484:410-415.
15. Joseph JM, Destaillats H, Hung H, Hoffmann MR. The sonochemical degradation of azobenzene and related azo dyes: rate enhancements via fenton's reactions. J. Phys. Chem. A. 2000; 104:301-307.
16. Kaneva N, Bojinova A, Papazova K, Dimitrov D. Photocatalytic purification of dye contaminated sea water by lanthanide (La^{3+}, Ce^{3+}, Eu^{3+}) modified ZnO. Catal. Today. 2015; 252:113-119.
17. Khodja AA, Sehili T, Pitichowshi JF, Boule P. Photocatalytic degradation of 2-phenylphenol on TiO_2 and ZnO in aqueous suspensions. J. Photochem. Photobiol. A. 2001; 141:231-239.
18. Korake PV, Dhabbe RS, Kadam AN, Gaikwad YB, Garadkar KM. Highly active lanthanum doped ZnO nanorods for photodegradation of metasystox. J. Photochem. Photobiol. B. 2014; 130:11-19.
19. Li L, Pan SS, Dou XC, Zhu YG, Huang XH, Yang YW, *et al*. Direct electrodeposition of ZnO nanotube arrays in anodic alumina membranes. J. Phys. Chem. C. 2007; 111:7288-7291.
20. Lin SH, Chen ML. Treatment of textile wastewater by chemical methods for reuse. Water Res. 1997; 31:868-876.
21. Marci G, Augugliaro V, Munoz MJL, Martin C, Palmisano L, Rives V, *et al*. Preparation, characterisation and photocatalytic activity of polycrystalline ZnO/TiO_2 systems. part 1. surface, bulk characterisation and 4-nitrophenol photodegradation in liquid-solid regime. J. Phys. Chem. B. 2001; 105:1033-1040.
22. Oliveira DP, Carneiro PA, Sakagami MK, Zanoni MVB, Umbuzeiro GA. Chemical characterization of a dye processing plant effluent–identification of the mutagenic components. Mutation Research: Fund. Mol. Mech. Mut. 2007; 626:135-142.
23. Pala RGS, Metiu H. The structure and energy of oxygen vacancy formation in clean and doped, very thin films of ZnO. J. Phys. Chem. C. 2007; 111:12715-12722.
24. Pareek VK, Adesina AA. Handbook of Photochemistry and Photobiology, ed. By Nalwa HS, American Scientific Publishers, Stevenson Ranch, CA. 2003; 1:345-412.
25. Raza W, Haque MM, Muneer M. Synthesis of visible light driven ZnO: Characterization and photocatalytic performance. Appl. Surf. Sci. 2014; 322:215-224.
26. Roosta M, Ghaedi M, Shokri N, Daneshfar A, Sahraei R, Asghari A. Experimental design based response

surface methodology optimization of ultrasonic assisted adsorption of safaranin o by tin sulfide nanoparticle loaded on activated carbon. Spectrochim. Acta, Part A. 2014; 122:223-231.

27. Selvam NCS, Vijaya JJ, Kennedy LJ. Comparative studies on influence of morphology and La doping on structural, optical, and photocatalytic properties of zinc oxide nanostructures. J. Colloid and Interface Sci. 2013; 407:215-224.

28. Senthilvelan S, Chandraboss VL, Karthikeyan B, Murugavelu M, Loganathan B, Natanapatham L. Novel sol-gel synthesis of cerium-doped ZnO thin films for photocatalytic activity. AIP Conference Proceedings. 2012; 1461:395-398.

29. Sobana N, Swaminathan M. The effect of operational parameters on the photocatalytic degradation of Acid Red 18 by ZnO. Sep. Purif. Technol. 2007; 56:101-107.

30. Suwanboon S, Amornpitoksuk P, Bangrak P, Muensit N. Optical, photocatalytic and bactericidal properties of $Zn_{1-x}La_xO$ and $Zn_{1-x}Mg_xO$ nanostructures prepared by a sol–gel method. Ceram. Int. 2013; 39:5597-5608.

31. Tavakkoli H, Moayedipour T. Fabrication of perovskite-type oxide $La_{0.5}Pb_{0.5}MnO_3$ nanoparticles and its dye removal performance. J. Nanostructure Chem. 2014; 4:116-124.

32. Van der Zee FP, Bouwman RHM, Strik DP, Lettinga G, Field JA. Application of redox mediators to accelerate the transformation of reactive azo dyes in anaerobic bioreactors. Biotechnol. Bioeng. 2001; 75:691-701.

33. Van der Zee FP, Villaverde S. Combined anaerobic–aerobic treatment of azo dyes: A short review of bioreactor studies. Water Res. 2005; 39:1425-1440.